QTL MAPPING OF STEM BIOMECHANICAL TRAITS AND PRECISION PHENOTYPING IN BIOENERGY SORGHUM

A Dissertation

by

FRANCISCO ERNESTO GOMEZ

Submitted to the Office of Graduate and Professional Studies of
Texas A&M University
in partial fulfillment of the requirements for the degree of

DOCTOR OF PHILOSOPHY

Chair of Committee,	William L. Rooney
Committee Members,	John Mullet
	Anastasia H. Muliana
	Scott A. Finlayson
Head of Department,	David D. Baltensperger

December 2017

Major Subject: Plant Breeding

ABSTRACT

Mechanical characterization is an important and now frequently used tool for phenotyping plants for crop improvement, e.g. lodging resistance. Mechanics of materials and structures in response to various external stimuli as well as information of basic building blocks that constitute the plants can be applied to study the mechanical behavior of plant stems. The inherent mechanical properties of plant structures such as the stem are relevant to breeding strategies, aiming to tackle issues such as crop lodging due to stem or root lodging. While empirical tests of breaking strength and stiffness have been applied to plants, few of these studies consider the genetic background of the plants examined. In this study, we report for the first time on the mapping of QTL for mechanical traits in sorghum in three RIL mapping populations from crosses between grain and sweet sorghum parents. The genetic architecture of biomechanical traits in the three RIL populations appear to be quantitative and pleiotropic. Six QTL affecting mechanical and morphological traits were detected; two of these QTL were consistently found in all populations and co-localized with previously cloned dwarfing genes *Dw1* and *Dw3*. These results suggest that dwarfing genes affect the mechanical properties of sorghum and ultimately their lodging resistance while also having a profound impact on the stem's morphology and geometry. Morpho-anatomical stem properties are major component affecting standability. However, phenotyping these traits is low throughput, and has been restricted by the lack of a high-throughput phenotyping platform that can collect both morphological and anatomical stem properties. X-ray computed tomography (CT) offers

a potential solution, but studies using this technology in plants have evaluated limited numbers of genotypes. The platform and image analysis pipeline revealed extensive phenotypic variation for important morpho-anatomical traits in well-characterized sorghum genotypes at suitable repeatability rates. CT estimates were highly predictive of morphological traits and moderately predictive of anatomical traits. The image analysis pipeline also identified genotypes with superior morpho-anatomical traits that there were consistent with ground-truth based classification in previous studies. In addition, stem cross section intensity measured by the CT was highly correlated with stem dry weight density, and can potentially serve as a high-throughput approach to measure stem density in grasses.

DEDICATION

To Maria and Francisco, my parents who introduced me to the joys of understanding the world, with gratitude and admiration and love. Also to my sister for her guidance and to Alicia for all her love and support throughout our graduate years.

ACKNOWLEDGEMENTS

First and foremost, I would like to thank my committee chair, Dr. William Rooney for giving me the support, trust and freedom to work throughout my training as a plant breeder and scientist. I would also like to thank my other committee members Dr. Anastasia Muliana, for her patience in teaching me a new subject and always willing to discuss science and mechanics with me. Dr. John Mullet for allowing me to work in his lab and discuss my research and always having an intuitive response to my questions. Dr. Scott Finlayson, for his inputs throughput my research and excellent plant physiology course which allowed me to learn more about thigmomorphogenesis in plants. Dr. Karl Niklas from Cornell University for his friendship and mentorship throughout my graduate career and introducing me to plant biomechanics.

Thanks also to my colleagues and the faculty and staff from the Texas A&M Sorghum Breeding Program for making my time at Texas A&M University a great experience.

CONTRIBUTORS AND FUNDING SOURCES

This work was supervised by a dissertation committee consisting of Dr. William Rooney of the Department of Soil and Crop Sciences and Dr. Scott Finlayson of the Department of Soil and Crop Sciences, Dr. Anastasia Muliana of the Department of Mechanical Engineering, and Dr. John Mullet of the Department of Biochemistry and Biophysics. Part of the data analyzed for Chapter 3 was provided by Dr. Geraldo Carvalho Jr of the Department of Soil and Crop sciences and image processing algorithm was conducted by Dr. Fuhao Shi of the Department of Computer Science.

This work was supported by the Texas A&M University Louis Stokes Bridge to Doctorate Fellowship VII Award (No. 1249272) for graduate fellowship and financial support granted to F.G. This was also funded by the Great Lakes Bioenergy Research Center.

TABLE OF CONTENTS

Page

LIST OF FIGURES

Page

LIST OF TABLES

Page

CHAPTER I

INTRODUCTION

Plant stems fulfill an array of functions to ensure the survival and competitiveness of a given plant species in its respective environment (Speck and Burgert 2011). One important function of stems is to provide mechanical support under static and dynamic loadings throughout their growing period. However, many plants including crop species are particularly susceptible to lodging due to wind loads. Lodging can take the form of stem or resulting from breakage, or root lodging due to failure of root anchorage (Berry et al. 2004). Lodging is essentially a structural failure; therefore, mechanical characterization of plants is an important tool to phenotype plants. Thus, inherent mechanical properties of the plant stems are relevant to agricultural studies (Gomez et al. 2017) that aim to reduce crop loss due to lodging by uprooting or stem breakage (Crook and Ennos 1996). However, there has been little selective breeding of crops for desirable mechanical properties because new unconventional methods and convergent interdisciplinary and disciplines are required to develop the tools that are to be used in a field breeding program.

During the 1960's the stems of wheat and rice were not strong enough to support the heavy grain of the high-yielding varieties after the application of large amounts of fertilizer and pesticides, resulting in lodging. This led to the introduction of dwarfing genes into these cereal crops and the technological advancement known as the 'Green Revolution' (Hedden 2003). The genes responsible for the semi-dwarf varieties are the *Reduced height* (*Rht*) genes in wheat and the *semidwarf1* (*sd1*) gene in rice. However,

despite the height reduction conferred by these genes, lodging in many of the cultivars carrying these genes remains a problem. Similar observations have been observed in the highly productive C_4 tropical grass sorghum (*Sorghum bicolor* L. Moench), where dwarf varieties carrying the dwarfing genes (*Dw*) occasionally have been known to stem lodge. Furthermore, stem lodging has also been observed in tall sweet, forage, and biomass varieties were height reduction is not viable as it would impact yield. Therefore, sorghum breeders improving lodging resistance in tall sorghum types have selected genotypes that do not lodge, as well as increased stem diameter and have not selected for mechanical properties. Thus, studying the stem's mechanical properties may provide for an alternative approach to conventional methods.

While several studies have quantified the mechanical properties of stems of important crops (Robertson et al. 2017; Crook and Ennos 1994; Oladokun and Ennos 2006) including sorghum (Lemloh et al. 2014; Bashford et al. 1976), only a few studies have taken into account the genetic background of the plants examined. However, these few studies have shed light into the genetics of mechanical traits of cereal grasses. For example, in rice, (Ookawa et al. 2010) identified a quantitative trait loci (QTL) for stem strength, which was identical to the ABERRANT PANICLE ORGANIZATION1 (APO1) gene previously reported to control panicle structure. The same group identified QTL for section modulus on chromosomes 1, 5, and 6 (Ookawa et al. 2016). In maize, (Hu et al. 2013) identified QTL for stalk bending strength parameters that were also highly heritable. While Paolillo Jr and Niklas (1996) reported the effects of reduced-height alleles of *Rht1* and *Rht2* on the breaking strength and breaking stress of the first leaves of wheat seedlings.

They found a negative correlation between *Rht*-dosage and breaking strength. Overall these studies led us to understand that QTL for mechanical properties are complex, pleiotropic, and that dwarf genes in wheat may influence the mechanical and materials properties of plants. However, to date no studies have looked at the genetics of biomechanical properties in sorghum, which could aid breeders to select for lodging resistant varieties.

Stem morphology has a profound impact on mechanical traits, and should also be considered when assessing mechanical stability in plants (Von Forell et al. 2015; Niklas and Spatz 2012). However, phenotyping bioenergy sorghum is slow and tedious. Improving the throughput of phenotyping would help accelerate these protocols to evaluate more plants. Currently the plant sciences are undergoing a high-throughput phenotyping revolution and image analysis is at the forefront of this revolution. High throughput methods to image plants will aid phenotyping. In addition, the combination of biomechanics and x-ray computed tomography have assisted to study bone biomechanics in other clinical studies in humans. This approach can be also applied to plants to identify new traits that can be used to indirectly select mechanical traits.

To understand the genetic architecture of biomechanical properties in sorghum and to help reduce the phenotypic bottleneck in bioenergy sorghum, we conducted experiments to; (1) develop a practical high-throughput phenotyping platform and image data processing pipeline that can phenotype many samples to extract stem morpho-anatomical properties and (2) perform a multi-trait QTL analysis to investigate the genetic basis of mechanical traits.

CHAPTER II

RAPID PHENOTYPING OF SORGHUM STEM PROPERTIES USING X-RAY COMPUTED TOMOGRAPHY

Introduction

Breeding for standability and yield is a major focus of sorghum geneticists and breeders (Mullet et al. 2014; Rooney et al. 2007). Stem biomechanical and morpho-anatomical properties affect standability (Niklas 1992; Esechie et al. 1977; Ookawa et al. 2010; Hu et al. 2013; Piñera-Chavez et al. 2016) and yield components in bioenergy sorghum (Carvalho and Rooney 2017) by influencing the plant's ability to resist lodging and produce juicy and large stems. However, using existing assays to measure stem biomechanical and morpho-anatomical traits demands significant amounts of labor and time which reduce throughput. New high throughput and advanced imaging technology provides a solution to alleviate this phenotyping bottleneck (Furbank and Tester 2011). This will ultimately enable plant scientist and breeders to evaluate larger segregating populations, which would improve the selection process.

X-ray computed tomography (CT) has become a powerful tool for phenotyping plants, and is becoming more widely available to a steadily growing number of plant biologists. As a result, this has led to vast amounts of image data which need to be efficiently managed, processed, mined, and analyzed (Chen et al. 2014; Bucksch et al. 2017; Metzner et al. 2015). Despite increasing interest in scanning plant stems using CT

(Comparini et al. 2016; Dhondt et al. 2010; Robertson et al. 2017), there have been few studies to visualize and quantify in a high throughput manner above-ground structures of plants in a high-throughput manner using CT.

To date, CT studies have used small sample sizes that limit the throughput and applicability of this method in large-scale field-breeding labs. For example, the high resolution X-ray CT (HRXCT) has been the CT scanner of choice in the plant sciences because of its high-resolution (Dhondt et al. 2010). The HRXCT uses state-of-the-art detector arrays and more powerful X-ray sources (up to 420 kV) than medical CT does; giving it increased spatial resolution to a few tens of microns [μm] (Stuppy et al. 2003). Depending on the resolution, the size of the sample, and desired signal-to-noise ratio, a CT scan may take several minutes to hours, and there is a sample size trade off (Tracy et al. 2017; Cloetenes et al. 2006; Bucksch et al. 2017). Therefore, the HRXCT works best on relatively small numbers of samples, which decreases the throughput of the technology. Diverse plant biology studies have used the HRXCT as a means to characterize the rhizosphere, roots, seeds, flowers, wood, and more at a very detailed level (Cloetenes et al. 2006; Kaminuma et al. 2008; Pajor et al. 2013).

In clinical research, a combination of biomechanics and X-ray CT has proven to be a powerful research technique to study whole-bone biomechanical properties (Keaveny 2010; Berger 2002). Application of such technology to crop improvement could be valuable as well. A study in maize successfully applied an HRXCT to generate structural morphology of dry maize stems, which were then implemented in finite-element (FE) analyses. FE analyses performed to study the biomechanical response of these stems

discovered that stem strength was highly dependent on stem morphology (Von Forell et al. 2015). The same group were able to scan up to 10 samples per run using HRXCT. Robertson et al. (2017), also using HRXCT, identified a relationship between stem morphology and biomechanics in late-season stem lodging in maize.

In bioenergy sorghum, stem lodging tends to occur at the grain filling stage (Gomez et al. 2017) when there is significant moisture and turgor pressure that may affect biomechanical properties (Niklas and Spatz 2012). As tissues mature and subsequently dehydrate as a result of senescence, the modulus of elasticity of these stem increases (Niklas 1992). Moreover, since bioenergy sorghum stem weight and moisture are good predictors of juice yield (Carvalho and Rooney 2017), it is important to evaluate plants when the physiological influences on the expression of these traits are minimal. Thus, previously mentioned results for late-season stem lodging in maize may not apply to bioenergy sorghum.

The current technological limitations of the HRXCT for acquiring plant morphological and anatomical data makes its application impractical in a field-breeding program. To be useful, the technology must have higher throughput even if resolution drops. To address this problem, we proposed the use of the Multi-Slice CT (MSCT) to visualize and quantify phenotypic data in a high throughput fashion that would allow scanning larger samples and increase the number of grass stem samples per run. Since an important goal of plant biology is to map genotype to phenotype (Chen et al. 2014), high-throughput genotyping and phenotyping platforms must work parallel with each other.

A robust stem phenotyping platform would mitigate a phenotyping bottleneck impacting bioenergy/forage sorghums. The platform should accurately estimate stem geometry and morpho-anatomical traits, allow for a large sample size, produce acceptable repeatability for the traits, and work quickly with minimal effort. Thus, the objectives of this study were to develop a practical high-throughput phenotyping platform and image data processing pipeline that can phenotype a large number of samples to extract stem morpho-anatomical properties and to validate the methodology.

Material and Methods

Plant material

Two different sets of sorghum germplasm were used in the study. Set 1 consisted of 19 genotypes including elite lines and cultivars which contrasted for maturity, stem morphology, stem anatomy, and end-use; while Set 2 consisted of ten F_2 plants derived from a cross between GIZA114 and Umbrella showing contrasting morpho-anatomical characteristics (Table A-1). All genotypes were evaluated to assess the potential of using a Multi-Slice CT (MSCT) to estimate stem properties in a field based breeding program. The pipeline for analysis of high-throughput phenotyping morpho-anatomical traits using CT is described in (Fig. 1).

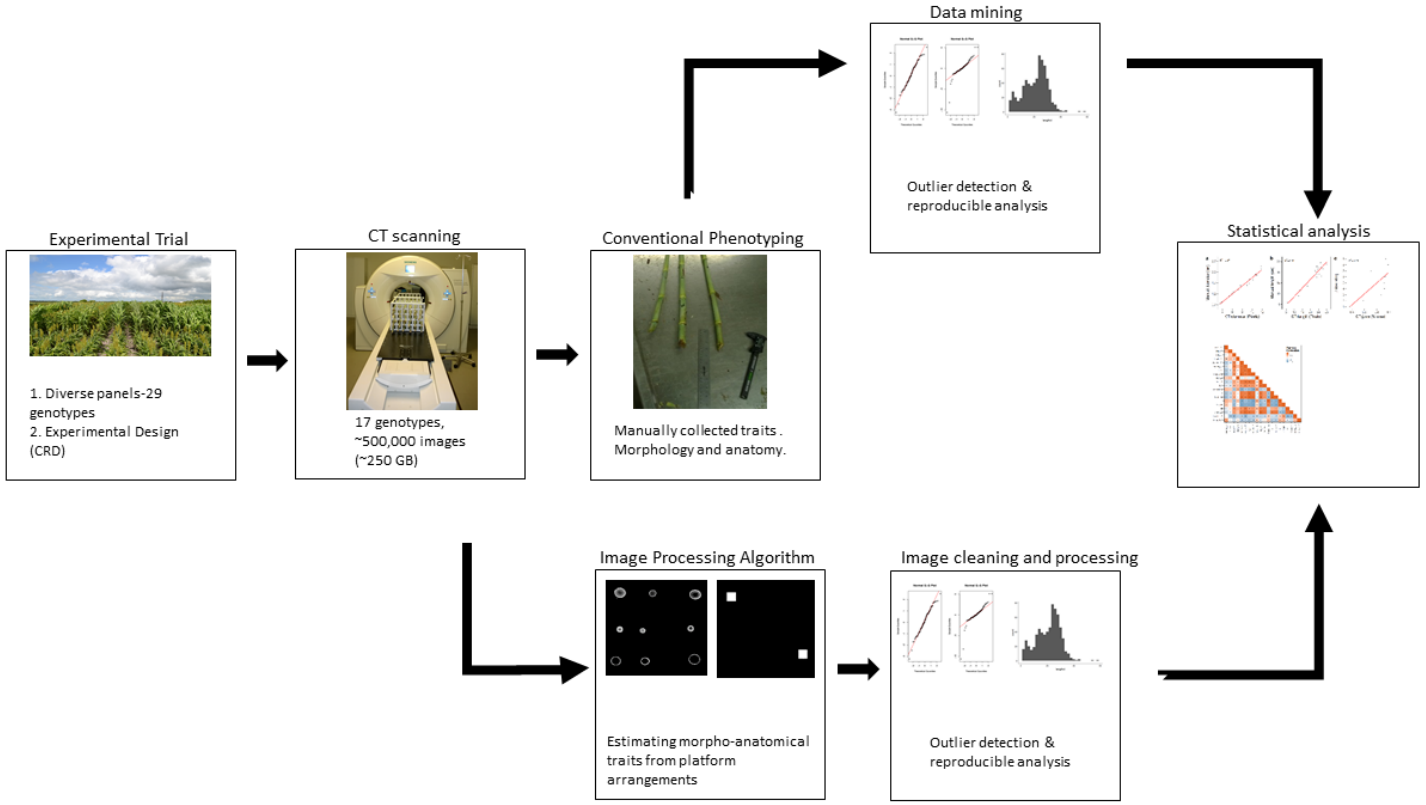

Fig. 1 Pipeline for analysis of high-throughput phenotyping in sorghum using a computed tomography and conventional phenotyping (see Methods).

Experimental details

Two separate field experiments were conducted in 2015 in College Station, Texas (30°32'31.6"N 96°25'21.6"W). Seeds were planted in one-row plots 5 meters long and 0.76 meters wide. Genotypes from Set 1 were arranged in a complete randomized block design. The target plant density was ~75,000 plants ha^{-1}. For Set 2, F_2 seeds were distributed in plots laid out in a row-by-column design. Seeds from Set 1 and Set 2 were sown in April. Agronomic practices standard for sorghum production in this area were used including irrigation as needed to minimize drought stress. Harvesting and evaluations occurred in July, approximately 95 days after planting.

For phenotyping each genotype in Set 1, six healthy plants were randomly selected from the middle of the plot and cut at the soil level. For Set 2, ten F_2 plants were randomly selected from a ten plot population block. After harvest, any growth greater than 1.5 meters was removed to fit because stem lodging in sorghum occurs primarily between internodes three and six (which are typically between 0.5-1.5 meters) (Gomez et al. 2017). For most samples, the remaining section included internodes 1-7 and some genotypes had >7 internodes in the 1.5 m section. This procedure was followed by the removal of leaf sheaf across the stem to get precise stem diameter measurements. During this time, plants were kept in a temperature-controlled environment at ~20°C and then transported to be scanned.

Phenotyping platform setup and CT-measurement

Multi-slice computed tomography (MSCT) is a clinical scanner used to test human or animal patients with a larger sample space that allows more samples per run. All

harvested plant samples were loaded on a platform that held 30 samples per scan (Fig. 1). X-ray CT scans were completed within an hour after harvest at the Diagnostic Imaging & Cancer Treatment Center of the Texas A&M Veterinary Medicine & Biomedical Sciences facilities in College Station, Texas. A SOMATOM Definition AS+ CT instrument (SIEMENS) was used with the following settings using 120 kVp, 1.024 pixels per mm, at a 0.6 mm slice thickness.

Morphological measurements

In Set 1, stem morphological traits were collected on the 1.5-meter section scanned in the CT analysis (Table A-1). Each internode was numbered, with the lower number closer to the base of the plant. The distance between each node was recorded as internode length (cm), and internode diameter (mm) was measured at the center of each internode using a digital caliper. Internode volume was estimated using the formula.

$$v = \pi r^2 h \quad [1]$$

where r is the radius of the stem, and h is the length of the internode. Internode fresh mass was taken for each internode using a digital balance (model 95364, CEN-TECH ®). Internode mass density was calculated using the formula

$$\rho = \frac{m}{v} \quad [2]$$

where, m is mass (g), and v is the volume of the internode. Samples were dried in a forced-air oven at 60° for one-week post phenotyping to estimate dry internode weight and density.

Stem biomechanics

Biomechanical properties were collected on the previously described samples. All internodes were cut at the nodes and were subjected to a three-point bending test (3PBT) following the methods described in Gomez et al. (2017). Biomechanical properties were determined based on the Euler Bernoulli beam theory since the tested internodes were relatively slender. The following formula calculated the dimensionless slenderness ratio (dimensionless)

$$\lambda = \frac{L}{D} \quad [3]$$

where *L* is the length of the stem section and *D* is the diameter of the stem section. A slenderness ratio >10 was maintained on all specimens.

The second moment of an area (*I*) quantifies the resistance to bending provided by cross-sectional geometry and size. The stem cross-section was approximated as a circular cross section. For beams with a solid circular cross-sectional geometry, *I* is given by the formula

$$I = \frac{\pi D^4}{64} \quad [4]$$

where *D* is the diameter of the stem section. The geometric property for a given cross section or section modulus (*Z*) was also calculated by

$$Z = \frac{I}{r} \quad [5]$$

where *I* is the second moment of an area and *r* is the radius of the internode. The elastic (Young's) modulus *E* reported in MPa is the quotient of normal stress to normal strain

throughout the linear range of elastic behavior (Niklas 1992), henceforth referred to as "material stiffness". *E* is given by

$$E = \frac{F_1 {L_{in}}^3}{48\, B_1\, I} \quad [6]$$

where B_1 is the lateral displacement it took to bend the stem section without damaging its structural integrity. F_1 is the force required to bend the stalk to displacement B_1, L_{in} is the length of the stem section, and *I* is given by Eq. [4]. In Eq. [6]. The measured elastic modulus is along the longitudinal axis of the stalks and the stalks are assumed as homogenized structures. It should be noted that stalks are heterogeneous structures, they are anisotropic with regards to the mechanical properties, and their overall mechanical responses are typically inelastic. However, as a first step in analyzing biomechanical properties of sorghum stalks, this study considers linear elastic response of stalks.

Stalk strength was taken as the maximum stress required to break the structural integrity of the stem (Niklas 1992) and is given by

$$\sigma_{max} = \frac{(F_2)L_{in}}{4I} * r \quad [7]$$

where F_2 is the force required to induce breakage, L_{in} is internode length, *r* is internode radius, and *I* is the second moment of an area (Eq. [4]). Flexural rigidity (herein referred to as rigidity), symbolized as *EI* is given by

$$EI = E * I \quad [8]$$

where *E* is stiffness and *I* is second moment of an area, and represents the resistance of a beam to bending forces based on size, geometry and material properties (stiffness). Plants are composite materials; therefore, the calculated biomechanical properties are interpreted as spatially averaged Young's modulus (Hesse et al. 2016; Rowe et al. 2006) and effective flexural rigidity across the entire heterogeneous plant tissues (Schulgasser and Witztum 1997; Wagner et al. 2012).

Anatomical measurements

Visual stem pithiness measurements from Carvalho and Rooney (2017) were used as these data included the same genotypes that were in Set 1. In brief, the percent of pithy stem cross section area was visually estimated by using a rating scale system. This scale ranges from 1 to 9, where one corresponds to 90-100% pithiness and 9 to 0-10% pithiness. One unit increase in the scale equals to 10% decrease in the percent of the pithy area. For Set 2, the same protocol was followed, but in this case, measurements were taken in the same plants scanned in the CT, and on internodes 3 and 6 only.

Computational image analysis

A customized computer program was written in in the MATLAB environment (Mathworks, Inc., Natick, MA, USA) to extract morpho-anatomical attributes from CT cross-section images. For the algorithm developed, the input is an image, and output is the region centers, diameters, rind area, cross section intensity, and percent pithy area. The process consisted of the following steps. First, we performed a morphological closing

operation to connect some disconnected regions due to the image noise. Then, isolated regions were extracted using the MatLab routine “regionprops”. Small regions, not part of the platform (areas that were below a preset threshold) were excluded. Additionally, a circle was fit for each remaining region. If the eccentricity for a region was too low (which means the region was not a circle), this region was not included in the analysis.

Next, we extracted the region center, diameter, rind area, area intensity, and pithy area for each remaining circle-like region. The circle center and diameter were saved as the region center and diameter. The density was measured as the ratio of the mean pixel intensities of a region and the max possible intensity of the image (which is 255). The rind area was defined as the area of the outer region. The inner circle was obtained by firstly excluding the pixels with intensities greater than a threshold (175), and then fitting the circle using the remaining pixel locations in that region. Finally, the percent pithy area was defined as the ratio between dark pixels (intensity is below a threshold, which is 20) inside each region and the area of the entire inner circle.

In total, over six morphological attributes were determined for each cross-section. Since it was not possible to detect nodes using the algorithm, node sections of the stem were added manually to the output. A separate function estimated internode length by multiplying the slice thickness of the CT image and the number of images within an internode section.

Image preprocessing

A total of ~500,000 images were produced by the CT scanning of ~150 plants. Figure S1 and Video S1 show arrangements and illustration of the 3D-reconstructed sorghum stems in the platform used to estimate morpho-anatomical traits. The pre-processing of phenotypic data involves removal of node sections since no data was collected at the nodes as well as regions where no data was estimated by the algorithm (i.e. 0). Missing estimates along the stem may have occurred when the stems move out of the area of estimation, or the algorithm did not detect a circle. Outlier detection was also performed.

Statistical analysis

First, individual data points estimated by the algorithm were averaged by internode. Next, the observed values for the morpho-anatomical traits were analyzed using a linear model, written as

$$y_{ij} = \mu + g_i + i(g)_{j(i)} + \varepsilon_{ij} \quad [9]$$

where μ is the grand mean, g_i is the fixed effect of the genotype, $i(g)_{j(i)}$ is the fixed effect of the internode number within the genotype, and ε_{ijk} is the random error component. LSMeans and standard errors were estimated for each genotype using the linear model. Pearson correlation coefficients where estimated using the LSMeans from the model for all manual and CT traits collected. The same model was run as a mixed model, except all

terms were random using the restricted maximum likelihood method (REML) to estimate the repeatability on a plot mean basis as follows:

$$H^2 = \frac{\sigma_G^2}{\sigma_G^2+\sigma_E^2} \quad [10]$$

where σ_G^2 is the genotypic variance and σ_E^2 is the error variance, respectively (Hallauer et al. 2010). For percent pithy area, plot mean values from Set 1 were combined with plant-based values from Set 2 to estimate repeatability and for modelling analysis.

A univariate regression was performed for internode diameter, length, and pithiness to study the relationship between CT-derived and manually collected stem traits. Three predictive models were fit to validate the accuracy and usefulness of the results. In the first model, the CT-derived internode diameter predicts the diameter collected manually; Diameter = Diameter CT. In the second model, CT-derived internode length predicts the internode length collected manually; Length = Length CT. In the third model, the CT-derived internode percent pithy area predicts the visual pithiness ratio; Pith = Pith CT. The performance of the models from the univariate regression was assessed by the leave on out cross-validation (LOOCV) method. For this, the data was split into two parts, and a single observation (x_1, y_1) was used for the validation set, and the remaining observations $\{(x_2,y_2),\ldots,(x_n,y_n)\}$ made up the training set. The statistical learning method was fit on the n-1 training observations and a prediction $\hat{y}$ was made on the excluded observation using its value x_1. The root mean square error (RMSE) of prediction was estimated for each validation, $RMSE_1$, $RMSE_2$, … , $RMSE_k$:

$$RMSE = \sqrt{\frac{1}{n}\sum(y - \hat{y}\,)^2} \qquad [11]$$

where y and $\hat{y}$ are the observed and predicted values in the model. The model acceptability was examined by the average of these n test error estimates.

The models were further evaluated by the proximity of the predicted versus observed values to the 1:1 line for each model and by identifying the lowest RMSE from the LOOCV. An R^2 value close to 1.0 with a slope of observed versus predicted close to 1.0 and small RMSE values indicate that the model is precise with little bias (Alam et al. 2016).

Results

Phenotypic variation for CT estimated traits was detected

Phenotypic variation existed among genotypes for all CT-derived traits. In Set 1, the genotypic LSMEANS across all internodes and plants ranged from 3.6 to 28 pixels for internode length; stem diameter ranged from 3.5 to 12 pixels; stem pixel intensity ranged from 0.61 to 0.83, and stem rind area ranged from 37 to 248 pixels. In the entire panel (Set 1 and Set 2 together), percent pithy area ranged from 11% to 60% on a mean genotype basis. The CT estimates effectively identified groups of genotypes with common phenotypes (Fig. 2). On average, the late maturing genotypes had the largest internode length, diameter, and rind values (Table A-1, Fig. 2a, 2b, 2e). Earlier genotypes showed higher stem intensity values (Table A-1, Fig. 2d) with a few exceptions, notably Tx14323, and GIZA114.

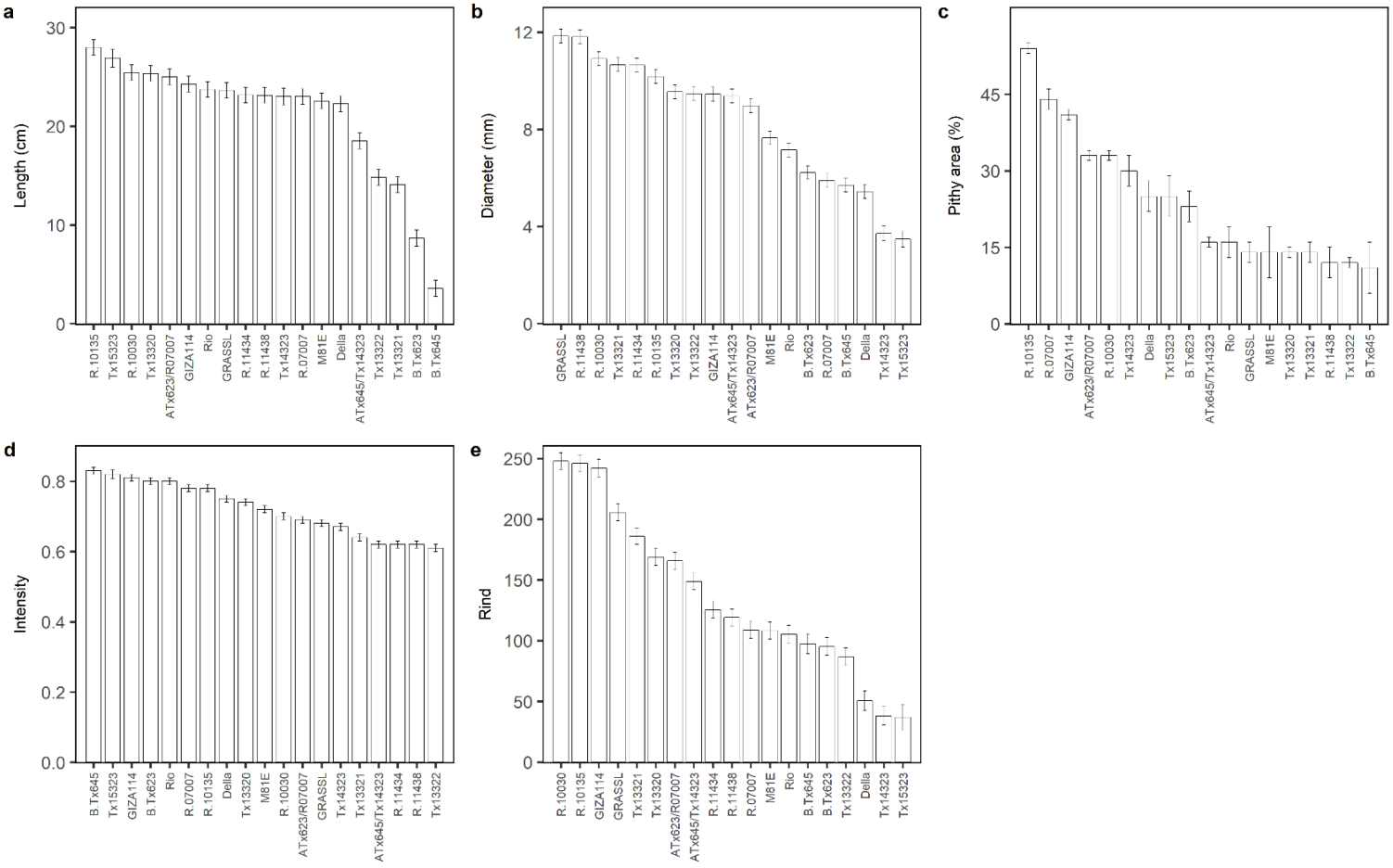

Fig. 2 Phenotypic variation for morpho-anatomical traits for 19 genotypes from Set1. Genotypes have been sorted by specific trait. The vertical bars indicate the relevant standard error; a) length (cm) b) diameter (mm) c) pithy area (%) d) intensity e) rind area

Repeatability for CT estimates trait

Repeatability estimates for CT-derived traits ranged from 0.51 to 0.72 and repeatabilities for manually collected traits ranged from 0.66 to 0.85 (Table 1). In most cases the CT-estimated traits were lower than the ground-truth trait estimates. High repeatabilities (~.70) were observed for rind, diameter, and volume, followed by length and intensity at 0.61, and by percent pithy area and second moment of an area, at 0.56 and 0.51, respectively. Overall, H^2 for CT and manually collected data were consistent with one notable exception. Overall, the repeatability is lower for the CT collected data.

Table 1 Repeatabilities for CT-derived traits and manually collected traits measured in 29 diverse sorghum genotypes.

	CT	Manually Collected
Trait	H^2	H^2
Internode length	0.61	0.76
Internode diameter	0.70	0.81
Internode volume	0.71	0.83
Second moment of an area (*I*)	0.51	0.66
Intensity	0.61	NA
Pithiness	0.56*	0.85*
Rind	0.72	NA

*Measured at individual plant basis
NA: data was not collected manually for this trait.

Accuracy of estimating morpho-anatomical traits of sorghum using x-ray computed tomography in sorghum

The coefficients of determination of genotypic CT mean values regressed to genotypic manually collected means were high for morphological traits and moderate for one anatomical trait (Fig. 3). For length and diameter, the R^2 were 0.91 and 0.97, respectively. Moreover, for percent pithy area the R^2 was 0.49; although this value was

lower than the ones observed for stem length and diameter, the algorithm was still capable of explaining 50% of the total variation for stem pithiness. The LOOCV applied at the individual internode data point basis (genotype vs. plant vs. internode) revealed average R^2 and RMSE values of 0.56 and 3.75 for internode length, respectively. For internode diameter, an average R^2 of 0.54 and an average RMSE of 2.78 was observed. For pithiness ratio, the average R^2 was equal to 0.44 while an average RMSE of 1.63 was found.

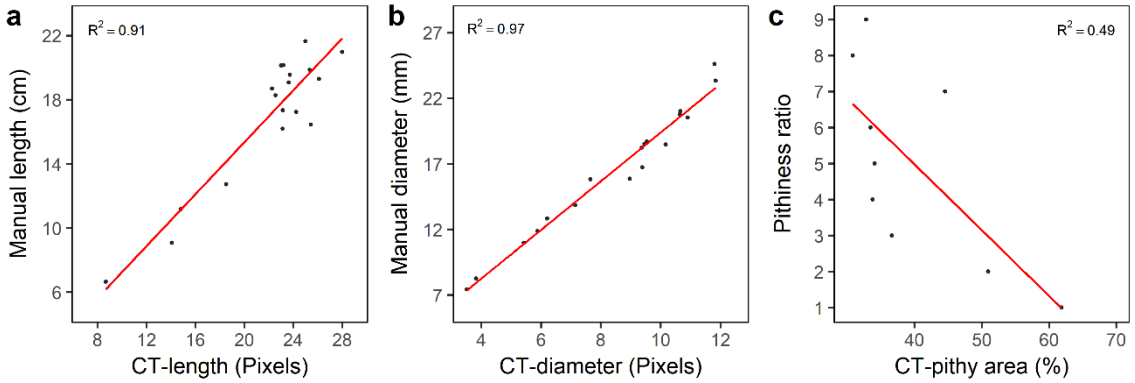

Fig. 3 Association between CT and manually collected traits for 29 sorghum genotypes; a) length b) diameter c) pithy area (%)

The adequacy of the predictive models were assessed by plotting predicted vs. observed (manually phenotyped) internode length, stem diameter, and pithiness ratio for all observations. Figure 4 shows the observed and predicted values for the model with the lowest RMSE selected from the LOOCV. The lowest RMSE for stem length, stem diameter and stem pithy area were 0.01, 0.02, and 0.02, respectively. The values for all three models were relatively precise and accurate across all observations. Furthermore, a 50% cut off line for the trait was added to evaluate the model as a selection tool in a sorghum breeding program (Fig. 4). The cut off separated the plots into four quadrants.

The quadrants with the blue observations were classified as the individual internodes that would be correctly classified using the model selected for each of the three traits. The accuracy of the model on classifying the values for the internodes of each genotype for stem length, diameter, and pithiness ratio was 81%, 77%, and 82%, respectively (i.e., from the total number of data points predicted, 81%, 77%, and 82% would be classified correctly upon selection for internode length, diameter, or pithiness).

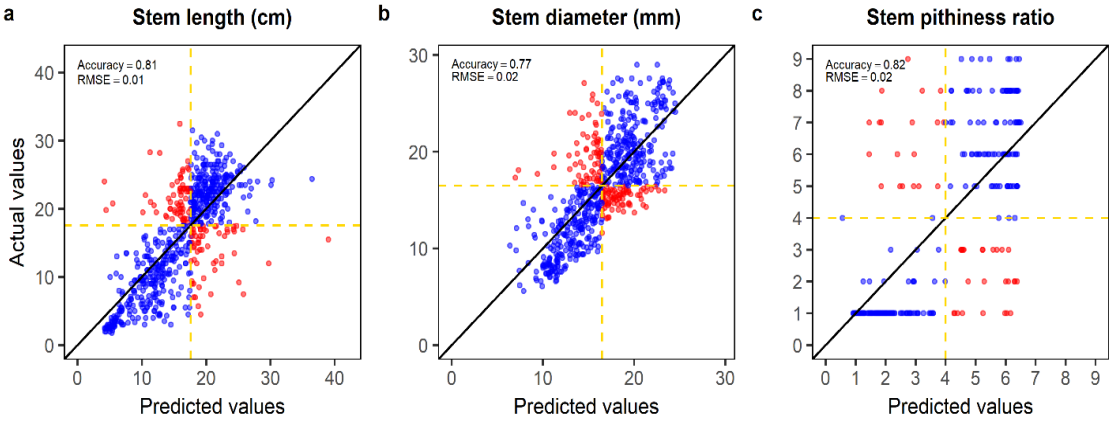

Fig. 4 Predicted versus observed plots for three traits and the model with the lowest RMSE select using the LOOCV method. Yellow line depicts a 50% cut off; a) stem length b) stem diameter c) stem pithiness ratio

Correlations among CT-derived traits

Correlations between CT-derived traits and morpho-anatomical manually collected traits were variable (Fig. 5). For example, CT and manual measurements of internode volume, internode fresh weight and dry weight were highly correlated. As expected, stem intensity was correlated with internode dry weight density (r=0.61; P<0.01), but percent pithy area-CT had very low correlations with the manually collected measurements. Rind-CT had a moderate correlation with section modulus and rigidity,

and a high correlation with volume-CT; (r=0.55; P<0.001), (r=0.66; P<0.005), (r=0.82; P<0.0001).

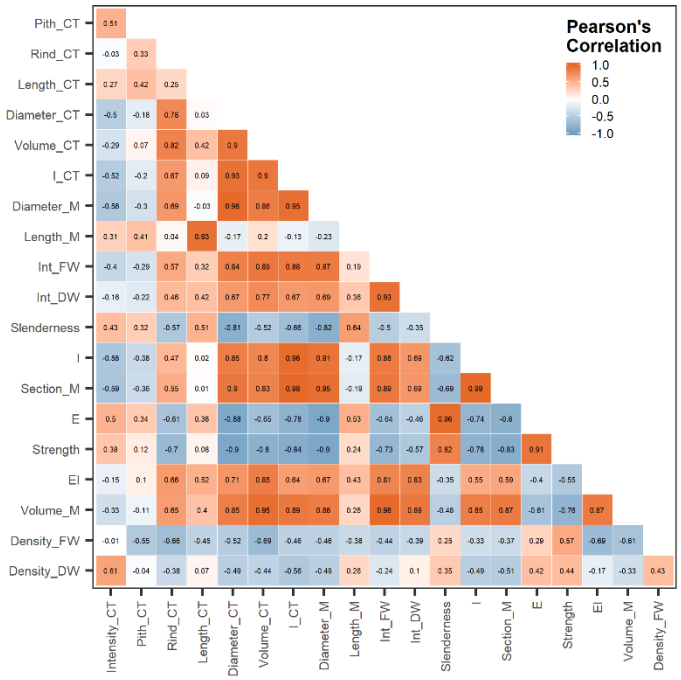

Fig. 5 A heatmap depicting Pearson's correlation coefficient for all traits collected in 19 sorghum genotypes from Set1.

Volume-CT was highly correlated with rigidity (r=0.85; P<0.001), respectively. Diameter-CT was positively correlated with rigidity (r=0.71; P<0.001) and negatively correlated with strength (r=-0.9; P<0.001) and stiffness (r=-0.88; P<0.001). These findings are consistent with results reported by Gomez et al. (2017).

Discussion

The phenotyping platform and algorithm presented herein were accurate and capable of detecting variation for important morpho-anatomical traits in well-characterized sorghum genotypes at reliable repeatability rates. The magnitude of the repeatability is a major factor in determining the efficiency and relevance of any phenotyping methodology in a germplasm screening program. In our case, repeatability estimates for CT-derived traits were moderate and were lower than manual measurements. The differences are likely due to minute variation present along the plant stem that could be captured by the CT method (Fig. 6) and cannot be assessed manually or visually. A single point manuallly collected measurement is likely to misrepresent the variation of each internode, which might cause an overestimation of variance when assessed across different plants and genotypes. Errors associated with the algorithm estimation might also be a complicator, but for this case, improvements are possible.

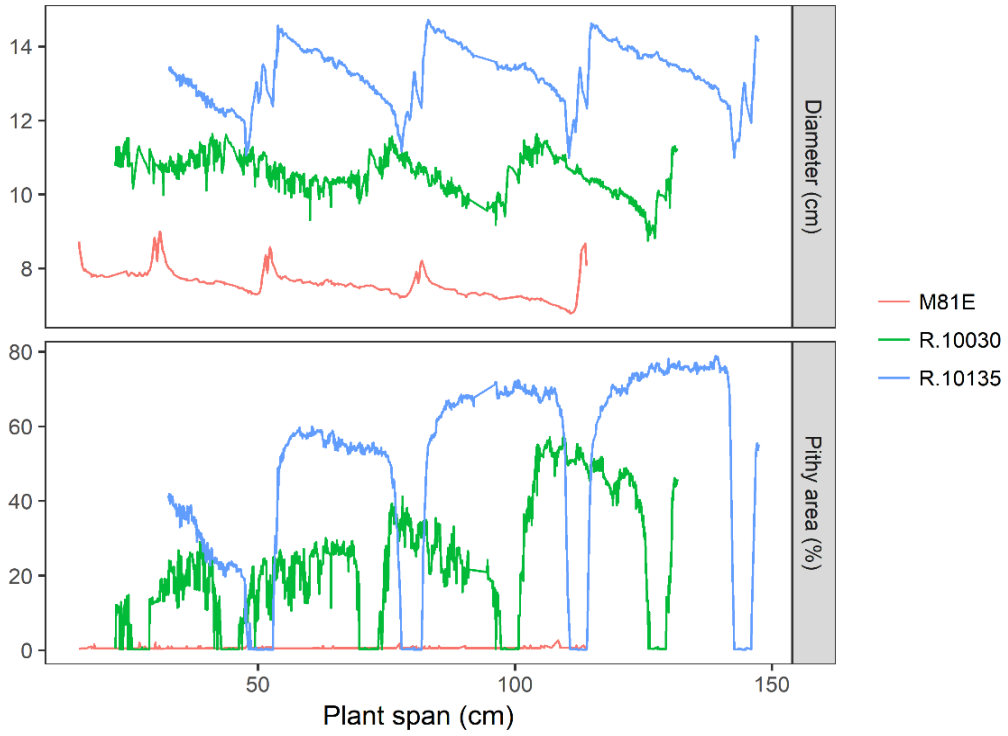

Fig. 6 Raw data from diameter and pithy area collected by CT for three sorghum genotypes plotted across the span of the plant stem. The drops at the graph represent zeros were the platform was removed.

Nonetheless, our image analysis pipeline could identify genotypes with superior morpho-anatomical traits that were consistent with manually based classification previously performed by Carvalho and Rooney (2017) and Gomez et al. (2017). For example, the genotype Rio had a smaller stem diameter than the genotype Tx13321 but longer internodes than Tx13321. The CT-estimated traits (internode diameter, internode length, and percent pithy area) were moderate to highly predictive of the manually collected traits. Although percent pithy area explained only 50% of the variation for pithiness rating, this may be a reflect inconsistencies in the visual score rather than, or in addition to, faults in the CT-based prediction. Visual ratings are one method to rate

pithiness, and it has been demonstrated that using a flatbed scanner can increase the accuracy of phenotyping (Carvalho and Rooney 2017). Therefore, an association between CT-derived percent pith and percent pith area estimations using a flatbed scanner might result in a higher association.

In this study, CT estimated morphological traits had the strongest correlations with mechanical properties. This finding is consistent with a computation sensitivity analysis in maize by Von Forell et al. (2015), demonstrating that morphological traits have a stronger association with mechanical traits rather than tissue or material properties. The results from the computation sensitivity analysis were also consistent with a study using CT to phenotype maize (Robertson et al. 2017). In our study, morphological measurements were also correlated with mechanical properties. For example, CT estimates of the second moment of an area were negatively correlated with stem strength and stiffness, demonstrating the strong effect stem morphology may have on mechanical traits. Similar results were reported by (Gomez et al. 2017). Furthermore, rind CT was moderately associated with section modulus and is in line with a study by Ookawa et al. (2016) where an *indica* variety of rice had strong culms due to a large section modulus that is associated with stem wall thickness. These results indicate that stem morphology has a strong effect on mechanical properties and morphological traits such as the second moment of an area and section modulus, and are to be considered when selecting for lodging resistance.

CT is based on the principle that the density of the tissue passed through by the X-ray beam can be measured by calculation of the attenuation coefficient (Lafond et al.

2015). Therefore, material density is a major factor to consider when running plant samples in a CT scanner, as plant organs vary in tissue density. This variation will affect the image from the CT scanners depending on the plant tissue's attenuation properties either soft tissue or hard tissue. Differences in X-ray attenuation in several plant stems were visibly apparent and primarily dependent on the anatomy, composition, and material density of the cross section of the stem (i.e. rind is more lignified) (Fig. S2). At this attenuation level obtained by the SOMATOM Definition AS+ it is possible to detect the material density of the stems as well as rind and pithy area. It has been shown that medical CT scanners capture the changes in material density and composition of relatively non-dense and large objects (Dutilleul et al. 2005; Lafond et al. 2015), such as stems of grasses. In this study, stem 'density' was estimated as the pixel intensities of a region and had high correlation with internode dry weight density. Other studies have provided similar results (Dutilleul et al. 2005). Therefore, intensity, as used in this study, is a new method to quantify stem density.

The need for a high-throughput method for quantifying important morpho-anatomical traits related to stem lodging and juice yield in bioenergy sorghum motivated this pipeline and platform. While many high throughput methods are being developed to phenotype plants using unmanned aerial vehicle (UAV), robotics, and high throughput platforms such as the ARPA-E TERRA-REF project (http://terraref.org/) (Watanabe et al. 2017; Andrade-Sanchez et al. 2014; Batz et al. 2016; Barker et al. 2016), none of these methods allow for combining external and internal stem phenotypic information of plants.

Besides the potential applications discussed for our pipeline, it can also be applied to produce highly dimensional data used in 3D reconstruction and crop modeling.

Image analysis is an active and challenging field of computer science that is rapidly providing tools applicable to biological problems. In principle, images can be mined for phenotypes other than those which were collected (Gehan and Kellogg 2017). In our study, images were mined to estimate morphological and anatomical properties effectively. However, the work herein is preliminary; there is room to improve on both processing and algorithms. For example, some of the coefficients of determination of the univariate regression did not explain all of the variation. We believe this was because plant stems vary in tissue density and the algorithm did not detect a complete circle, and therefore, did not estimate a value for that specific CT slice. Using methods such as machine-learning, algorithms to predict phenotypes in plant breeding programs can be improved.

The results indicate that CT-based estimates are associated with important traits in bioenergy sorghum. Furthermore, predicting traits such as stem length, diameter, and pithiness ratio at the internode level by utilizing HTP computed tomography appears possible in an applied breeding program. Further work to improve algorithms and the accuracy of our models will enhance the speed and efficiency of this methodology allowing it to be applied to large populations, panels, and hybrids with high fidelity. As a selection tool, our protocol appears readily applicable in field-based and large-scale breeding programs.

CHAPTER III

QTL FOR STEM BIOMECHANICAL PROPERTIES IN SORGHUM CO-LOCATE WITH DWARFING GENES

Introduction

Sorghum bicolor is a bioenergy feedstock that can be used to meet biofuel demands. Compared to grain sorghum hybrids, bioenergy sorghum hybrids are taller (3-4 meters) with longer internodes and greater biomass yield (15-40 Mg/ha depending on genotype and environment) (Mullet et al. 2014; Rooney et al. 2007; Gill et al. 2014; Hilley et al. 2016). These characteristics make them more susceptible to stem lodging.

The importance of breeding for lodging resistance has been a matter of prime importance for sorghum breeding programs since the 1940's (Karper and Quinby 1946) and continues to be so today. Grain sorghum breeders have indirectly selected for recessive alleles of *Dw1-Dw4* to prevent lodging and allow machine harvesting (Quinby 1974; Quinby and Karper 1953). Nevertheless, stem lodging continues to be a major problem reducing yield in grain and bioenergy sorghum. Furthermore, the use of dwarfing genes has been found to reduce shoot biomass and ultimately reduce grain yield (George-Jaeggli et al. 2011); therefore, breeders must understand the trade-off between reducing height and yield.

In rice, breeders have selected on recessive alleles in the gibberellin (GA)-related semi-dwarf plants during the Green Revolution (Hirano et al. 2014). However, increasing

the bending resistance because of the use of GA-related semi-dwarf traits does not necessarily result in increased lodging resistance. In addition, GA-dependent semi-dwarf plants have also lower grain yield (Okuno et al. 2014). While the *semi-dwarf1* (*sd1*) gene in rice (*Oryza sativa* L.) and the *reduced-height* genes *Rht1* and *Rht2* in wheat (*Triticum aestivum* L.) played a big roles in the green revolution to reduce lodging (Hedden 2003), varieties carrying these genes, are still affected by lodging (Ookawa et al. 2010). A more complete understanding of the genetic and biomechanical basis of stem lodging could identify ways to increase stem lodging resistance of bioenergy sorghum.

Biomechanical properties dictate the plant's mechanical integrity and these change as the plants mature and encounter environmental changes (Niklas 1992). Studies on important cereal crops have addressed the importance of biomechanical properties as means to improve lodging resistance. For example, in maize, Hu et al. (2013) found quantitative trait loci (QTL) using a three-point bending test (3PBT) which suggested a complex polygenic inheritance for stalk bending related traits. In rice, Ookawa et al. (2010) used a 3PBT test to identify a QTL labeled *STRONG CULM2* (*SCSM2*) from a high lodging resistant *Indica* cultivar Habataki, which was identical to the (APO1) gene which controls panicle structure. Ookawa et al. (2016) in rice also, confirmed a QTL in rice for section modulus on chromosomes 1, 5, and 6 of segment substitution lines (CSSLs) in reciprocal crosses between Koshihikari and Takanari.

A study by Paolillo Jr and Niklas (1996) assessed how the structural and material properties of wheat plants carrying the *Rht* alleles may effect field performance, and reported the effect of the *Rht* alleles on the breaking strength and breaking stress of the

first foliage leaves of the wheat seedlings. The study found that breaking strength increases with the cross-sectional area of cell walls in the principal fiber stands, and that the *Rht* allele changes the nature of this relationship such that a lesser increase in breaking strength per unit area of wall is attained in the presence of *Rht*. This study demonstrated that *Rht* may profoundly affect the morphology, development, and biomechanics of wheat. Like the *Rht* genes in wheat, the *Dw* genes in sorghum also affect stem morphology and ultimately the stem's biomechanical properties. Unfortunately, there is limited information regarding the genetic basis of stem biomechanical properties in sorghum and their association with important dwarfing genes important for lodging resistance. This information may aid breeders to exploit the genetic variation for these dwarfing genes.

The aims of this study were to map QTL for biomechanical traits in sorghum and assess potential relevance of the traits for improving lodging resistance via marker-assisted or genomic selection. To achieve this aim, in this study we 1) identify QTL for biomechanical and morphological traits using three RIL bi-parental mapping populations, 2) validate these QTL in different genetic backgrounds, 3) demonstrate that biomechanical traits QTL are associated with morphological traits, 4) determine where the biomechanical traits QTL are located and identify co-location with reported dwarfing genes.

Material and Methods

Genetic material

Three recombinant inbred line (RIL) mapping populations comprising of two subsets of ~70 $F_{2:4}$ RILs developed from crosses between the sweet sorghum cultivar

'Della' to both elite inbred parents 'BTx623' and 'BTx631', and ~100 $F_{2:5}$ RILs consisted from a cross between the sweet sorghum cultivar with juicy stalks 'Rio' with the elite inbred parent 'BTx623' (Table 2) (Murray et al. 2008) were used. The RILs were developed following head to row of individual F_2 plants to F_4 and F_5 respectively.

Table 2 Description of recombinant inbred mapping populations used in the three-point bending test experiments, planted in different environments at College Station, TX during 2014-2016.

Populations	Generation	RILn°	Replications	Environments
Tx623/Rio	$F_{2:5}$	97	2	3 (CSE2014, CSL2014, CSE2016)
Tx623/Della	$F_{2:4}$	70	2	3 (CSE2014, CSE2015, CSE2016)
Tx631/Della	$F_{2:4}$	72	2	2 CSE2014, CSE2016)

CSE: College Station Early, CSL: College Station Late.

Experimental design and sampling

The RILs and the parental lines were evaluated using a randomized complete block design over two seasons across years at two different locations in Texas at different planting dates to obtain three distinct environments (Table 2); College Station from April to July 2014-16 (CSE) and May to August 2014 (CSL). All mapping populations were manually thinned to a specific target population density of ~75000 plants/ha and tillers removed. Standard sorghum agronomic practices for each area were used including irrigation as needed to minimize drought stress.

Trait measurements were collected during the grain filling state, between internodes three and six, where stalk lodging is more prevalent (Gomez et al. 2017). Three healthy and randomly selected plants in the middle of the plot were cut at the soil level for phenotyping. RILs of similar height were sampled to minimize the confounding effect of

height on the biomechanical properties. Measurement on all plants were completed within 7 hours of harvest. Between harvest and measurement, the stalks were maintained in a temperature-controlled environment at ~21°C to minimize tissue dehydration and maintain natural material properties.

Phenotyping morphological and biomechanical traits

Prior to phenotyping all leaves and leaf sheaths were removed from each plant. Plant height was measured as the length (cm) of the plant from the base to the top of the panicle. After plant height was recorded, further data was collected on the region of the stalk between internodes three to five. These internodes were labeled with internode one, being the first internode above the ground. For internodes three to five, the distance between each node was recorded as internode length (cm) and internode diameter (mm) was measured at the center of each internode using a digital caliper. Internode fresh mass was taken for each individual internode using a digital balance (model 95364, CEN-TECH ®) to estimate internode mass density using the formula in Eq. [2].

Biomechanical properties in all environments were measured on the previously described samples using a three-point bending test protocol described in (Gomez, Muliana, et al., 2017). Biomechanical properties were determined based on the Euler Bernoulli beam theory since the tested internodes were relatively slender. The following formula calculated the dimensionless slenderness ratio using the formula in Eq. [3], where L is the length of the stem section and D is the diameter of the stem section. A slenderness

ratio >10 was maintained on all specimens. However, this parameter was not used for trait further trait analysis.

The second moment of an area (*I)* quantifies the resistance to bending provided by cross-sectional geometry and size. The stem cross-section was approximated as a circular cross section. For beams with a solid circular cross-sectional geometry, *I* is given by the formula in Eq. [4], where *D* is the diameter of the stem section. The geometric property for a given cross section or section modulus was also calculated by dividing *I* by *r* which is the radius of the internode. The elastic (Young's) modulus *E* reported in MPa is the quotient of normal stress to normal strain throughout the linear range of elastic behavior (Niklas 1992), henceforth referred to as "material stiffness". *E* is given by the formula in Eq. [6], where B_1 is the lateral displacement the stem section may undergo without damaging its structural integrity. F_1 is the force required to bend the stalk to displacement B_1, L_{in} is the length of the stem section, and *I* is given by Eq. [3].

Stalk strength was taken as the maximum stress required to break the structural integrity of the stem (Niklas 1992) and was calculated using the formula in Eq. [7], where F_2 is, the force required to induce breakage, L_{in} is internode length, *r* is internode radius, and *I* is the second moment of an area Eq. [3]. Flexural rigidity (herein referred to as rigidity), symbolized as *EI* was calculated by multiplying E by I Eq. [8] represents the resistance of a beam to bending forces, taking into account size, geometry and material properties (stiffness). Plants are composite materials; therefore, the calculated biomechanical properties are interpreted as spatially averaged Young's modulus (E)

(Hesse et al. 2016; Rowe et al. 2006) and effective flexural rigidity across the entire heterogeneous plant tissues (Schulgasser and Witztum 1997; Wagner et al. 2012).

Statistical analyses of phenotypic data

Genetic variation among RILs for each trait were assessed using linear mixed effects models at different environments and across environments for each population. Different mixed models using covariates and spatial models were compared with AIC and BIC; and the most appropriate model in each environment was used to obtain best linear unbiased estimates (BLUEs). BLUEs were used because values are not shrunken toward the mean, and thus, avoid artifacts arising from twofold shrinkage (Piepho et al. 2012). The final model of each individual environment was evaluated separately for each trait and included block and genotypes:

$$Y_{ij} = \mu + B_i + G_j + \varepsilon_{ij} \quad [12]$$

where Y_{ij} is the phenotypic value of genotype j in block i, μ is the overall mean, B_i is the block random effect $B_i \sim N(0,\sigma_b^2)$, G_j is the genotypic fixed effect, and ε_{ij} is the random error. Broad sense heritability (H^2) on an entry mean basis was estimated for analysis of individual experiments as $H^2 = \frac{\sigma_G^2}{\sigma_G^2 + \frac{\sigma_e^2}{r}}$ Eq. [13], where σ_G^2 and σ_e^2 are the genotypic and error variances, and r are the number of blocks (Hallauer et al. 2010).

Combined analysis across experiments was also performed using linear mixed effects model approach with unequal variances and a distinct residual variance for each

environment. The model included environment, replicates nested within environment, genotype, and genotype x environment interaction:

$$Y_{ijk} = \mu + G_i + E_j + GE_{ij} + B(E)_{k(j)} + \varepsilon_{ijk} \quad [14]$$

Here, Y_{ijk} is the phenotypic value of genotype i in environment j and block k; μ is the overall mean; G_i is the random effect of inbred line i and is ~ $N(0,\sigma_G^2)$; E_j is the effect of environment j, ~ $N(0,\sigma_{(E)}^2)$; GE_{ij} is the interaction between inbred line i and environment j and is ~ $N(0,\sigma_{GE}^2)$,; $B(E)_{k(j)}$ is the random block effect nested within each environment j and is ~ $N(0,\sigma_{B(E)_{k(j)}}^2\sigma_{B_k(E)})$, and ε_{ijk} is the random residual effect for inbred line i in the replication k of trial j and is ~ $N(0,\sigma_\varepsilon^2)$. Variance components were estimated for the model by treating all terms in the model equation as random effects exceptμ. Broad sense heritability (H^2) on a mean basis was estimated across environments as $H^2 = \frac{\sigma_G^2}{\sigma_G^2+\frac{\sigma_{GE}^2}{\eta}+\frac{\sigma_e^2}{r\eta}}$ Eq. [15], where σ_G^2 is the genotypic variance, σ_{GE}^2 is the genotype x environment variance, σ_e^2 is the error variance, and η and r are the number of environments and replicate plots, respectively (Hallauer et al. 2010). Models were fitted using the restricted maximum likelihood method. A principal component analysis (PCA) was carried out to get an overall picture of trait correlations using the R package FactoMiner. The predicted BLUEs from each of the traits for all populations were combined into a matrix and analyzed.

Molecular data collection and genetic map construction

Genomic DNA from individual inbred lines from the three populations (Table 2) was extracted from leaf tissue using the FastDNA Spin Kit (MP Biomedicals). Each inbred line was genotyped using Digital Genotyping (Morishige et al. 2013), using the enzyme *Fse*I (New England Biolabs) for digesting the genomic DNA. Libraries were sequenced with Illumina HiSeq2500 using standard Illumina protocols employed by Texas A&M AgriLife Genomic and Bioinformatics Services. FASTQ read files were obtained from Texas A&M AgriLife Genomic and Bioinformatic Services and processed using a series of custom Perl and Python scripts (Morishige et al. 2013). Reads were mapped to the *Sorghum bicolor* reference genome sequence (Sbi1) with the Burrow-Wheeler Aligner (BWA v0.7.5.a) (Paterson et al. 2009; Li and Durbin 2010)

A genetic linkage map composed of 10 linkage groups for all populations was constructed using JoinMap 4.1 software (Van Ooijen and Voorrips 2001). Loci that were 95% similar were excluded and segregation distortion was assessed using χ^2 against the normal Mendelian expectation ratios. Individuals markers that showed a significant linkage distortion where subsequently excluded from further analysis. To correct for crossover interference, the Kosambi mapping function was used to determine the genetic linkage distance in centimorgans (cM) (Kosambi 1943). The multipoint maximum likelihood ML based algorithm was used for map construction, and the Monte Carlo optimization method was used for estimating the 'best' map order.

QTL analysis

A mixed model multi-trait (MT) quantitative trait loci (QTL) mapping as described in (Malosetti et al. 2013; Malosetti et al. 2008) was performed, using the BLUEs for all traits for each environment. The strategy consisted of performing a genome-wide scan for QTLs by simple interval mapping (SIM), followed by several rounds of composite interval mapping (CIM) (using step size of 10cM) starting with cofactors selected from the SIM. Lastly, a final multi-QTL model was fit to estimate QTL effects.

Because target traits for QTL analysis are known to correlate with plant height (Blum et al. 1997; George-Jaeggli et al. 2011), an alternate QTL analysis was performed on the phenotypic data adjusted for plant height. BLUEs were estimated from the model in [Eq. 1] but adjusted for height. The QTL analysis was based on BLUEs adjusted for height was compared with the previous QTL analysis.

Results

Phenotypic trait variation

For most traits in all three populations the parents were significantly different than their RIL population in individual environments (Table 3). In general, the sweet sorghum parents were stiffer, stronger, and more rigid then the grain sorghum parents. The RILs exhibited transgressive segregation for biomechanical properties beyond the range of the parental values in all three populations at all environments. Estimates of genotypic effects were significant for almost all traits at individual environments (Table 4). Across locations genotype and genotype x environment interactions were significant for most traits.

Furthermore, genotypic variation accounted for the largest single source of variation for morphological and biomechanical traits in all three RIL populations, followed by the genotype x environment variance. For the Tx631/Della RIL population environmental and genotype x environment interaction accounted for very little of the variation in diameter, the two geometric properties, and the biomechanical properties. The results from the three RIL populations indicate that most biomechanical traits are strongly influenced by genetic factors, but are also subject to the interaction between genotype and environment.

Table 3 Predicted mean and range of three set of RIL populations and their parents for morphology and biomechanical traits.

			Morphology				Geometry		Biomechanics		
RIL	Environment	Parent or RIL	Plant Height	Int. Length	Int. Diameter	Int. Density	Int. Second Moment	Int. Section Modulus	Int. Strength	Int. Stiffness	Int. Rigidity
			cm	cm	mm	gcm-3			Mpa	MPa	Nm^2
B.Tx623/Della	CSE2014	B.Tx623	112 c	6.6 c	15.3 b	3.3 a	3145 b	380 b	7.2 b	43 a	0.1 c
		Della	322 a	19.5 a	18.6 a	1.2 b	5893 a	627 a	23.6 a	1214 a	7.2 a
		RILs	222 b	16.0 b	16.5 b	1.3 b	3366 b	401 b	25.2 a	1428 a	3.7 b
		Range	77-352	2.5-29.8	8.2-27.6	0.1-4.4	222-9730	54-922	3.4-52	3-5028	0.02-10.4
	CSE2015	B.Tx623	147 c	6.7 c	11.5 b	NA[a]	1161 b	175 b	34.5 a	1810 a	0.7 c
		Della	250 a	21.6 a	16.2 a	NA[a]	2254 a	304 a	39.4 a	2068 a	5.2 a
		RILs	214 b	15.4 b	13.0 b	NA[a]	1263 b	189 b	42.6 a	2326 a	2.7 b
		Range	104-338	1.3-30.5	4.8-25.1		26-3818	11-457	0.3-90.0	23-7081	0.1-7.8
	CSE2016	B.Tx623	129 c	8.9 c	15.2 a	1.3 a	2931 a	364 a	17.8 c	424 c	0.7 c
		Della	257 a	25.2 a	14.5 a	1.2 a	2449 a	319 a	25.7 a	2720 a	5.6 a
		RILs	220 b	20.0 b	14.8 a	1.2 a	2593 a	328 a	24.0 b	1904 b	4.1 b
	Range	99-335	3.0-33.5	4.4-24.9	0.5-11.3	18-8012	8-797	4.3-47.6	4-61	0.02-11.6	
B.Tx623/Rio	CSE2014	B.Tx623	112 c	5.3 b	16.1 a	3.5 a	3165 a	381 a	9.6 c	41 c	0.1 c
		Rio	265 a	17.9 a	14.8 a	1.5 b	2579 a	334 a	43.6 a	2301 a	5.1 a
		RILs	221 b	16.2 a	15.3 a	1.4 b	2926 a	364 a	31.0 b	1489 b	3.6 b
		Range	104-312	4.0-30.5	7.1-23.8	0.4-4.4	125-8012	35-797	2.9-62.9	15-4489	0.01-9.6
	CSE2016	B.Tx623	133 c	8.1 c	15.5 a	1.5 a	3342 a	396 a	17.2 c	469 c	0.7 c
		Rio	301 a	24.3 a	15.5 a	1.2 b	2864 a	366 a	33.4 a	2964 a	8.2 a
		RILs	244 b	19.9 b	15.2 a	1.2 b	2849 a	358 a	23.5 b	1758 b	4.2 b
		Range	104-328	2.0-34.8	7.7-23.0	0.5-5.1	173-7854	45-785	1.5-47.4	2-5702	0.003-12.1
	CSL2014	B.Tx623	113 c	5.2 c	16.5 a	3.2 a	4204 a	478 a	6.4 c	19 b	0.0 c
		Rio	327 a	17.9 a	16.5 a	1.2 b	4107 ab	470 ab	37.0 a	1485 a	4.6 a
		RILs	265 b	14.5 b	15.7 a	1.3 b	3225 b	392 b	28.7 b	1102 a	2.8 b
		Range	109-378	1.5-31.5	8.3-24.2	0.3-7.6	233-8840	56-858	1.2-70.9	2-3832	0.01-7.9
B.Tx631/Della	CSE2014	B.Tx631	113 c	5.5 c	19.3 a	3.5 a	7113 a	722 a	6.5 b	19 b	0.1 c
		Della	335 a	20.3 a	18.7 a	1.2 b	6676 a	677 a	23.1 a	1252 a	7.1 a
		RILs	233 b	15.4 b	17.3 b	1.3 b	4710 b	513 b	22.5 a	1078 a	3.6 b
		Range	85-395	2.0-29.8	7.5-30.7	0.5-7.7	155-13265	41-1164	1.6-45	2-3568	0.01-10.1
	CSE2016	B.Tx631	121 c	5.8 c	18.1 a	NA[a]	5688 a	603 a	8.2 c	16 c	0.1 c
		Della	252 a	23.3 a	16.0 c	NA[a]	3483 c	418 b	24.6 a	1867 a	6.0 a
		RILs	211 b	17.7 b	16.7 b	NA[a]	4129 b	464 b	21.9 b	1227 b	4.0 b
		Range	86-348	2.0-36.4	7.9-28.1		191-13737	48-1194	0.2-52.8	2-4510	0.02-11.6

BLUEs in column followed by the same letter are not significantly different from each other based on a Tukey's post hoc test at the 5% probability level.

Heritability estimates

Heritability estimates varied depending on trait, environment, and population (Table 4). For Tx623/Rio, the heritability estimates for biomechanical traits ranged from 51 to 78% in individual environments, while across environments ranged it from 74 to 90%. Heritability estimates for biomechanical traits for Tx623/Della in the individual environments ranged from 38% to 70%, while across environments it ranged from 73-86%. Lower heritability estimates were observed for the Tx631/Della population, where single environment heritability estimates ranged from 43 to 65%, and 82 to 85% across environments. This may also be attributed to the low variability of some of the morphological traits affecting the biomechanical traits as well.

Table 4 Variance components and heritability for individual trials and combined trials for all traits in thee RIL populations.

			Morphology				Geometry		Biomechanics		
RIL	Environment	Effect	Plant Height	Int. Length	Int. Diameter	Int. Density	Int. Second Moment	Int. Section Modulus	Int. Strength	Int. Stiffness	Int. Rigidity
BTx623/Rio	CSE2014	σ^2_g	91.7***	72.2 ***	58.9***	83.1***	47.0***	46.2***	56.0***	45.6***	63.8***
		σ^2_{error}	8.2	27.4	40.5	16.6	53.0	53.8	44.0	54.4	36.0
		$\boldsymbol{H^2}$	**96.0**	**84.0**	**74.0**	**91.0**	**64.0**	**63.0**	**72.0**	**63.0**	**78.0**
	CSL2014	σ^2_g	50.0***	51.4***	56.4***	NA[a]	51.1***	52.4***	43.5***	32.7***	43.9***
		σ^2_{error}	49.9	48.6	41.8	NA[a]	46.5	45.0	51.6	63.2	56.0
		$\boldsymbol{H^2}$	**67.0**	**68.0**	**72.9**	**NA[a]**	**66.7**	**67.9**	**62.8**	**50.8**	**61.0**
	CSE2016	σ^2_g	85.3**	62.2**	56.1**	15.1**	57.9**	57.3**	36.0**	40.5**	49.3**
		σ^2_{error}	13.7	37.6	43.9	84.3	42.1	42.7	63.9	59.2	50.5
		$\boldsymbol{H^2}$	**92.6**	**76.8**	**71.9**	**26.5**	**73.3**	**72.9**	**53.0**	**57.6**	**66.1**
	Combined	σ^2_l	20.32**	28.91**	0.17[ns]	4.05	1.22**	0.98[ns]	15.60*	16.46**	17.95**
		σ^2_g	65.86**	50.24**	28.59**	56.24	29.14**	28.27**	32.47**	34.89**	53.00**
		σ^2_{g*l}	4.52**	8.66**	4.73[ns]	14.31	4.30**	4.24[ns]	17.44**	9.97**	5.91**
		σ^2_{error}	9.22	11.37	64.15	23.85	63.32	64.24	32.84	36.46	23.12
		$\boldsymbol{H^2}$	**95.5**	**91.3**	**70.0**	**86.5**	**70.9**	**70.0**	**74.2**	**78.8**	**90.1**

[a] Data were not collected for this trait in this trial.

*Significant at the 0.05 probability level, ** Significant at the 0.01 probability level, *** Significant at the 0.001 probability level, ns=non-significant at 0.05 probability level.

Estimates of the RIL (σ^2_g), replicate (σ^2_r), location (σ^2_{lg}), interaction between the RIL and trial (σ^2_{g*l}), and the experimental error (σ^2_g), variances for each trial and combined for all traits collected.

Table 4 Continued.

RIL	Environment	Effect	Morphology				Geometry		Biomechanics		
			Plant Height	Int. Length	Int. Diameter	Int. Density	Int. Second Moment	Int. Section Modulus	Int. Strength	Int. Stiffness	Int. Rigidity
BTx623/Della	CSE14	σ^2_r	0.8	0.0	0.5	NA[a]	1.2	1.4	3.3	3.4	0.3
		σ^2_g	86.2***	64.4***	38.5***	NA[a]	33.8***	34.3***	51.7***	39.7***	56.4***
		σ^2_{error}	13.0	35.6	61.0	NA[a]	64.9	64.3	45.0	56.8	43.3
		H²	**90.0**	**80.0**	**60.0**	**NA[a]**	**50.0**	**50.0**	**70.0**	**60.0**	**70.0**
	CSE15	σ^2_g	86.7***	59.6***	36.6***	NA[a]	36.6***	35.9***	37.5***	36.6***	51.3***
		σ^2_{error}	13.3	40.4	63.2	NA[a]	63.3	64.0	62.5	63.4	48.6
		H²	**92.9**	**74.7**	**53.7**	**NA[a]**	**53.6**	**52.9**	**54.5**	**53.6**	**67.8**
	CSE16	σ^2_g	85.9***	34.1***	36.2***	NA[a]	33.0***	33.2***	28.9***	22.4***	31.5***
		σ^2_{error}	14.1	63.4	59.1	NA[a]	64.3	63.7	70.2	74.1	68.5
		H²	**92.4**	**51.8**	**55.0**	**NA[a]**	**50.6**	**51.0**	**45.2**	**37.7**	**47.9**
	Combined	σ^2_l	0.78[ns]	21.09**	25.70**	NA[a]	35.77**	37.33**	52.56**	18.44*	13.44**
		σ^2_g	65.97**	59.67**	35.96**	NA[a]	26.55**	27.67**	17.33**	40.65**	52.18**
		σ^2_{g*l}	13.82**	6.71**	10.61**	NA[a]	12.90**	10.58**	10.69**	3.50[ns]	14.84**
		σ^2_{error}	19.38	12.47	27.09	NA[a]	24.48	23.99	17.15	34.94	19.52
		H²	**89.4**	**93.3**	**81.7**	**NA[a]**	**76.0**	**78.6**	**73.0**	**85.3**	**86.4**
Tx631/Della	CSE14	σ^2_g	75.3***	58.9***	41.2***	44.1	36.9***	37.6***	44.2***	39.0***	47.5***
		σ^2_{error}	24.3	41.1	58.1	55.8	63.1	62.4	55.8	61.0	52.3
		H²	**86.1**	**74.2**	**58.6**	**61.2**	**53.9**	**54.6**	**61.3**	**56.2**	**64.5**
	CSE16	σ^2_g	69.5***	41.3***	44.4***	NA[a]	39.8***	40.8***	27.2***	26.1***	28.6***
		σ^2_{error}	25.6	41.2	42.9	NA[a]	49.2	47.8	72.8	62.2	69.5
		H²	**84.4**	**66.7**	**67.4**	**NA[a]**	**61.8**	**63.0**	**42.7**	**45.6**	**45.1**
	Combined	σ^2_l	8.51***	2.93***	0.00***	NA[a]	0.00***	0.00***	2.0	0.2***	0.34**
		σ^2_g	55.03***	41.24***	31.02***	NA[a]	25.51***	26.06***	27.15***	26.88***	34.59***
		σ^2_{g*l}	12.45***	5.26***	12.39***	NA[a]	13.40***	13.72***	6.30***	6.73***	4.79***
		σ^2_{error}	22.12	40.63	49.90	NA[a]	55.68	54.58	59.24	66.39	59.09
		H²	**82.4**	**76.3**	**62.4**	**NA[a]**	**55.3**	**56.0**	**57.0**	**60.2**	**66.8**

[a] Data were not collected for this trait in this trial.

*Significant at the 0.05 probability level, ** Significant at the 0.01 probability level, *** Significant at the 0.001 probability level, ns=non-significant at 0.05 probability level.

Estimates of the RIL (σ^2_g), replicate (σ^2_r), location (σ^2_{lg}), interaction between the RIL and trial (σ^2_{g*l}), and the experimental error (σ^2_g), variances for each trial and combined for all traits collected.

Trait correlations

The principal component analysis of trait values for Tx623/Rio showed that the first two principal components accounted for ~89% of the phenotypic variation (Fig. 6). The first PCA axis (Dim1) explained 57.3% of the total variation and was positively correlated with stiffness, strength, and internode length (Table A-2). Dim 1 was negatively correlated with internode density. The second axis (Dim2, r^2=31.8%) was positively correlated with section modulus and internode diameter, and second moment of an area. The principal component analysis for Tx623/Della summarized the traits into 2 principal components (Fig. 7) accounting for 95.17% of the phenotypic variation. The first PCA axis (Dim1) explained 57.54% of the total variation and was positively correlated with internode diameter, section modulus, and second moment of an area (Table A-3). The second axis (Dim2, r^2=37.63%) was positively correlated with plant height, internode length, and rigidity. The traits for Tx631/Della were summarized into 2 principal components (Fig. 8) accounting for 95% of the phenotypic variation. The first PCA axis (Dim1) explained 63.3% of the total variation and was positively correlated with stiffness, strength, and internode length (Table A-4). While other morphological and biomechanical traits were moderately positively and negatively correlated. The second axis (Dim2, r^2=31.75%) was positively correlated with plant height, rigidity, and internode length, but only moderately correlated with internode diameter, section modulus, and second moment of an area. Overall these results indicate that morphological and mechanical traits specifically internode length, strength and stiffness tended to group together, indicating a high correlation among them.

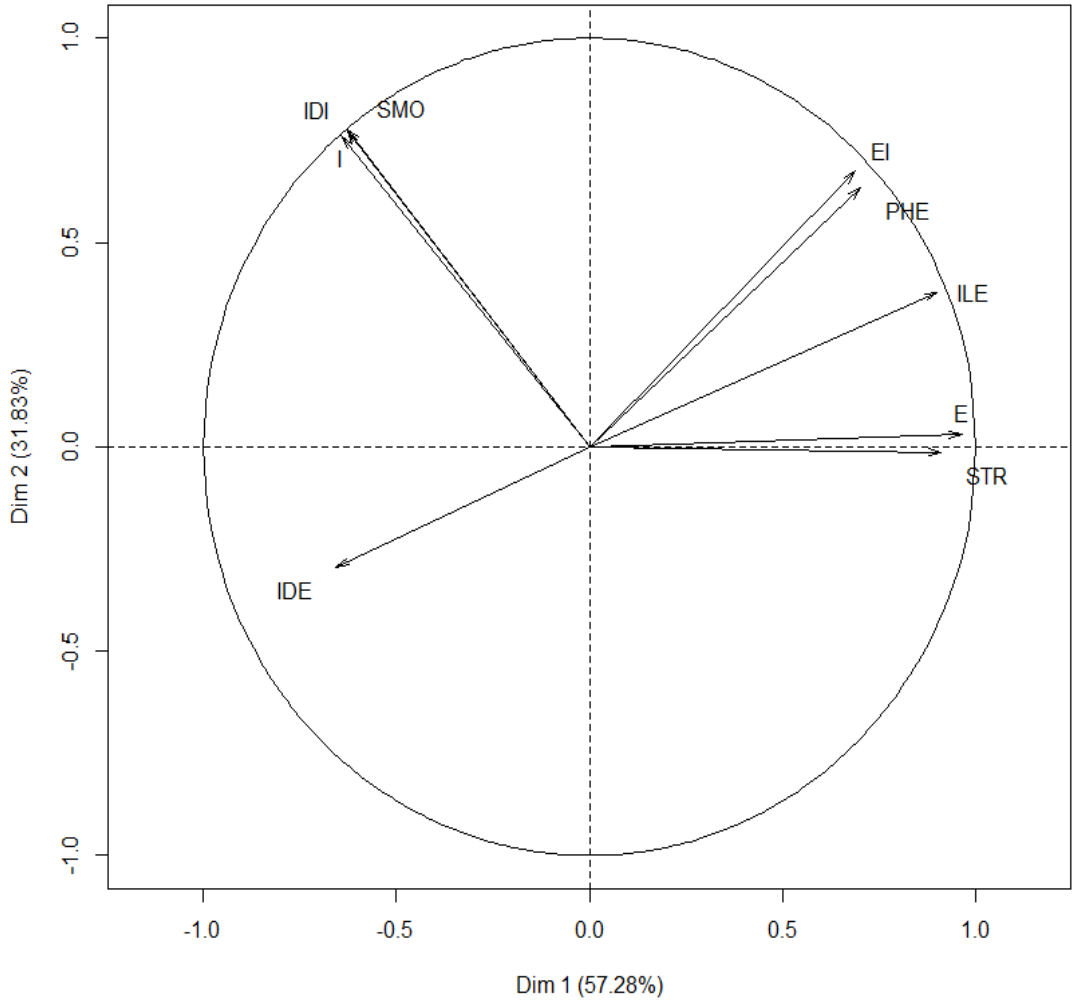

Fig. 7 Projection of traits on the two first PCA axes built with 9 traits for the Tx623/Rio Population; E) stiffness, EI) rigidity, I) second moment of an area, IDE) internode density, IDI) internode diameter, ILE) internode length, PHE) plant height, SMO) section modulus, STR) strength.

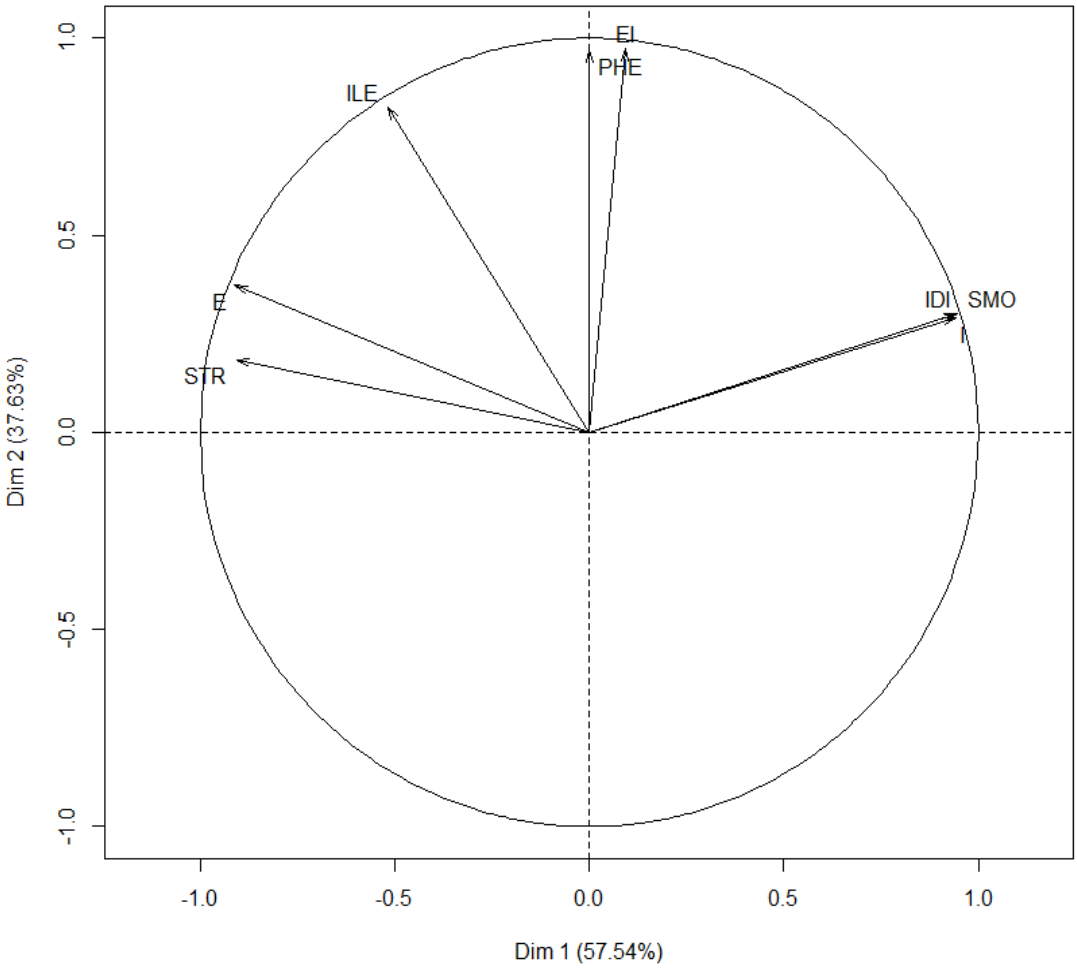

Fig. 8 Projection of traits on the two first PCA axes built with 9 traits for the Tx623/Della Population; E) stiffness, EI) rigidity, I) second moment of an area, IDE) internode density, IDI) internode diameter, ILE) internode length, PHE) plant height, SMO) section modulus, STR) strength.

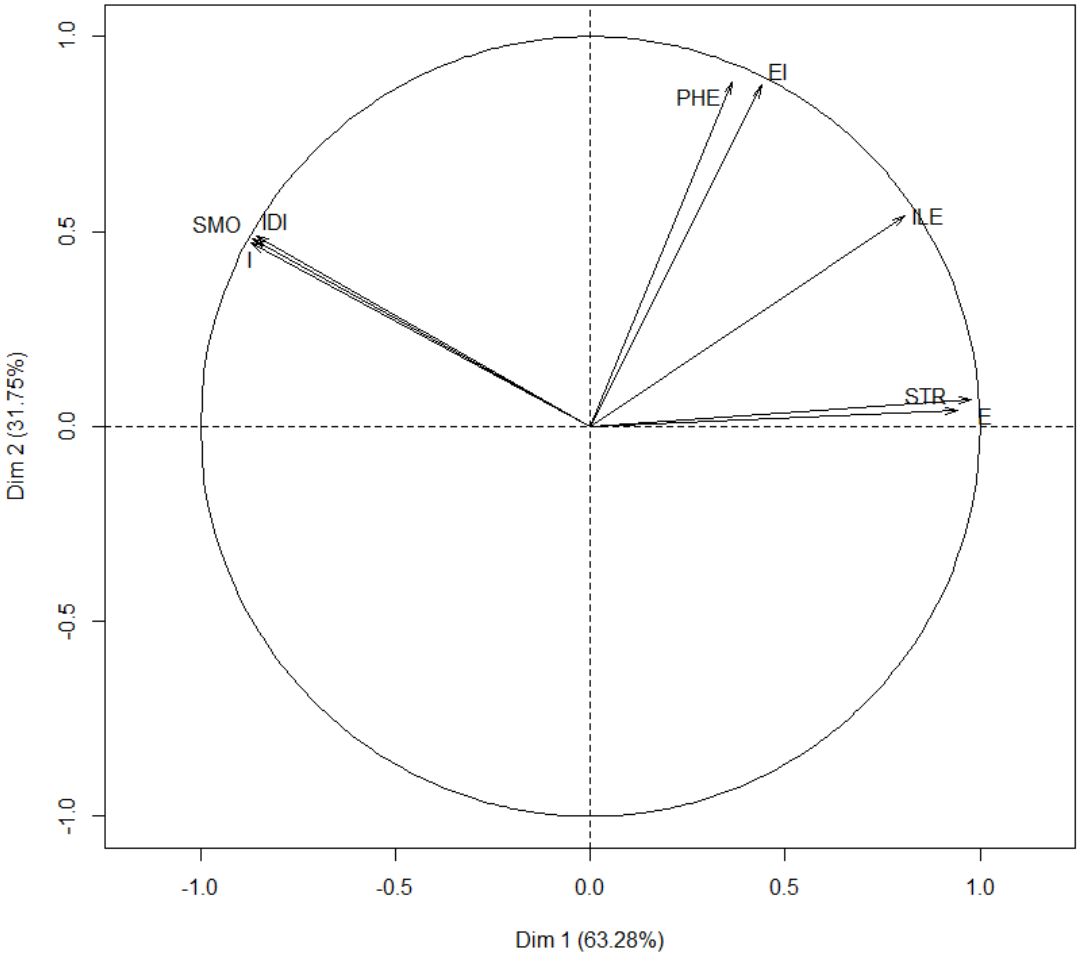

Fig. 9 Projection of traits on the two first PCA axes built with 8 traits for the Tx631/Della Population; E) stiffness, EI) rigidity, I) second moment of an area, IDI) internode diameter, ILE) internode length, PHE) plant height, SMO) section modulus, STR) strength.

Genetic linkage mapping

A recombinant map composed of 864 single nucleotide polymorphism (SNP) genetic markers distributed over 10 chromosomes was generated and used to conduct the QTL analysis for Tx623/Rio (Table 5 and Fig. 10). Overall the median distance between markers was 1.1 cM and the mean 95% percentile distances between markers was 6.2 cM. A total of 816 SNP markers were used to conduct the QTL analysis for Tx623/Della (Table 5 and Fig. 11). Here, the overall median distance between markers was 0.8 cM and a mean 95% percentile distance between markers was 5.9 cM. For the Tx631/Della population, a total of 1038 SNP markers were used create the map and conduct the QTL analysis (Table 5 and Fig. 12). On average, the distance between markers was 0.9 cM and a mean 95% percentile distance between markers was 5.9 cM.

Multi-trait QTL analyses and validation

The multi-trait QTL analysis conducted in individual populations and environments identified a total of eight genomic regions associated with mechanical and morphological traits on chromosome arms 1, 2, 3, 4, 5, 6, 7, and 9 (Table 6-8 and Fig. 13-15). The three genomic regions on chromosome 1, 7, and 9 were found to be repeatedly associated with morphological and mechanical traits in all three populations at most locations. Furthermore, two genomic regions on chromosome 4 and 6 were consistently found in two populations, while two minor effect QTL on chromosomes 2, 3, and 5 were only detected on individual populations.

Table 5 Genetic mapping statistics for three sorghum populations used in this study.

Population	Chromosome	Length	Number of markers	Median distance between markers	95% percentile distances
Tx623/Rio	1	209.1	147	1.0	4.5
	2	179.8	84	1.1	7.1
	3	193.7	133	0.9	4.6
	4	177.0	98	0.9	7.3
	5	163.4	64	1.5	8.6
	6	67.6	51	0.5	6.2
	7	135.8	48	1.2	14.6
	8	133.5	66	1.1	6.7
	9	133.7	84	1.1	5.2
	10	135.1	89	1.1	3.8
	Genome	1528.6	864	1.1	6.2
Tx623/Della	1	227.1	123	0.7	9.6
	2	125.9	113	0.8	3.3
	3	135.7	63	1	11.8
	4	163.6	143	0.7	3.5
	5	120.3	72	0.9	7.2
	6	62.9	60	0.7	3.2
	7	111.4	49	1.4	7.9
	8	125.5	48	1.7	7.9
	9	156.2	102	1	5.3
	10	65.5	43	0.8	4.4
	Genome	1294.1	816	0.8	5.9
Tx631/Della	1	275.2	190	1	4.7
	2	181.8	128	0.9	5.7
	3	53.2	55	0.7	2.8
	4	176.8	118	0.9	5.3
	5	161.3	91	0.9	5.2
	6	171.3	119	0.7	6
	7	222.6	49	3.1	13
	8	123.1	80	0.9	6.4
	9	133.2	103	0.6	6
	10	157.2	105	0.8	6
	Genome	1655.6	1038	0.9	5.9

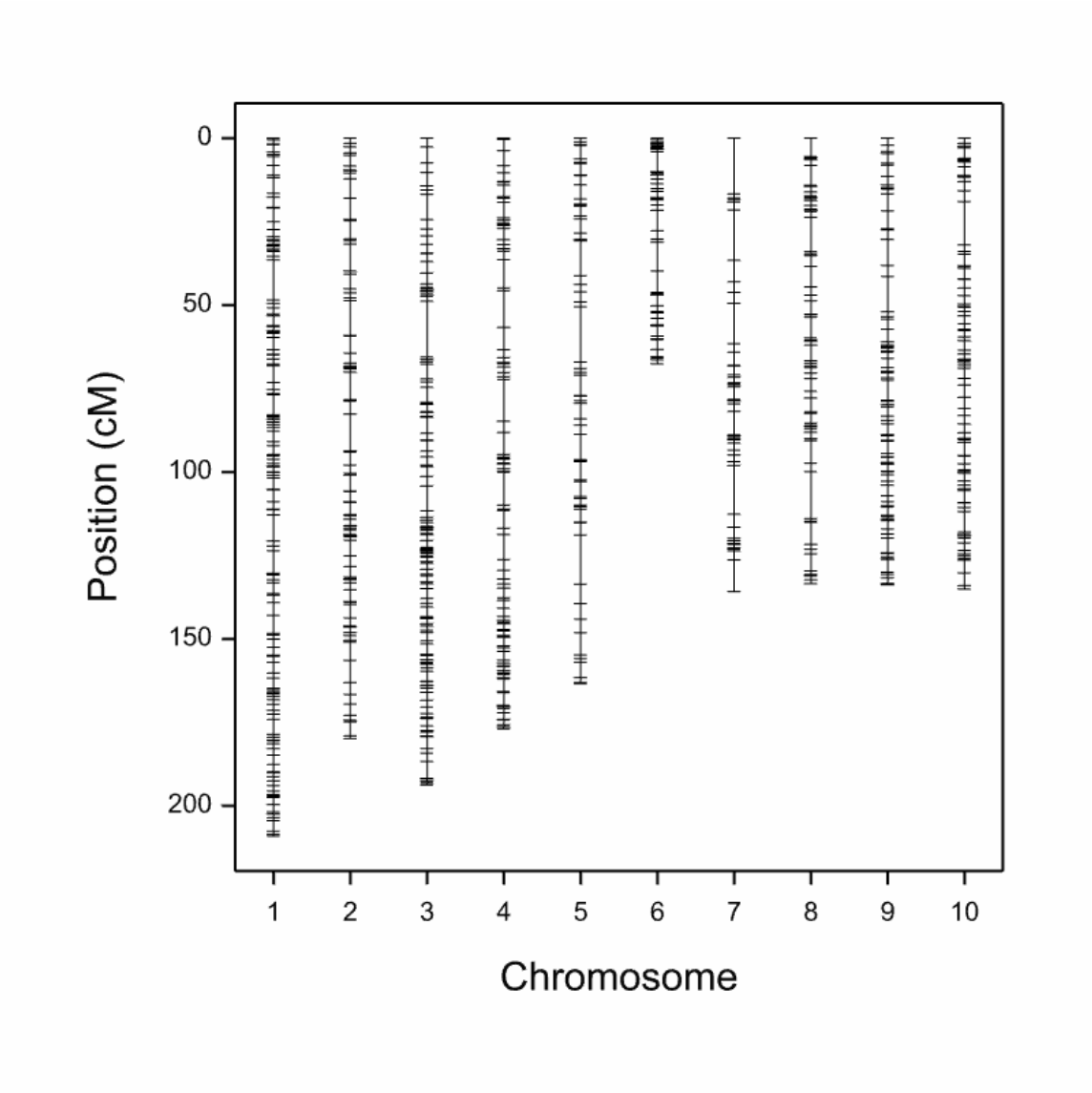

Fig. 10 Genetic Map for Tx623/Rio.

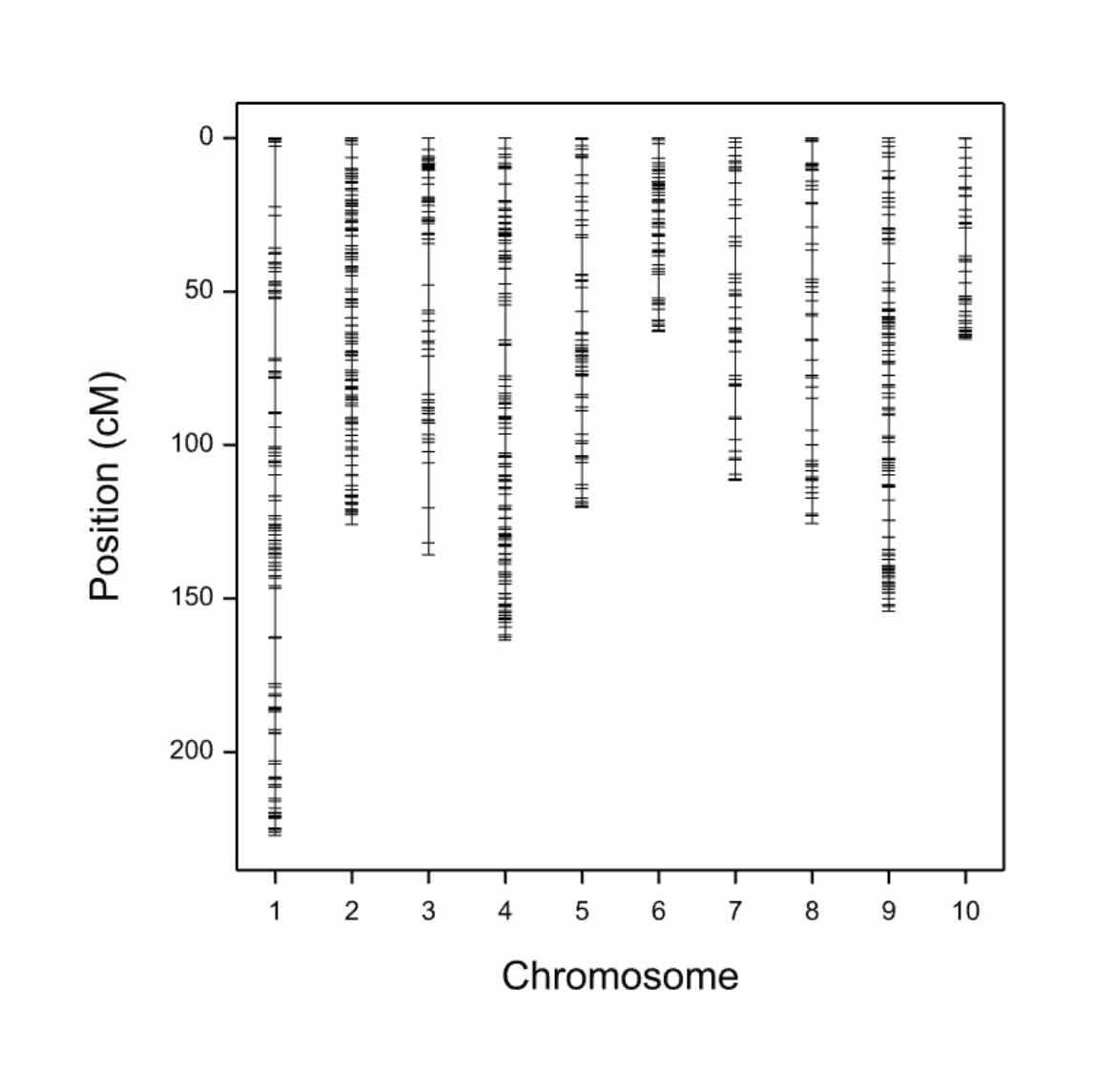

Fig. 11 Genetic Map for Tx623/Della.

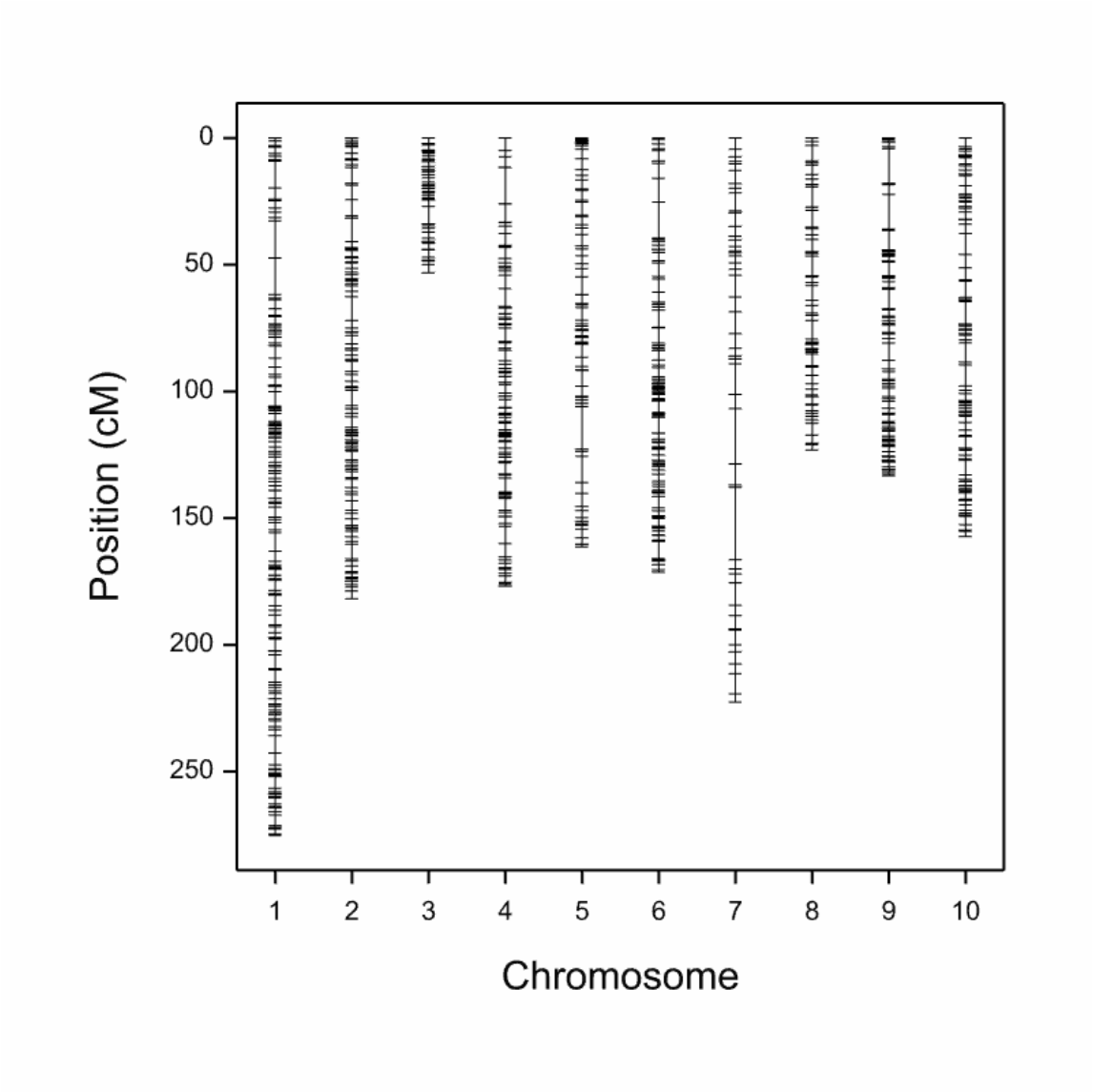

Fig. 12 Genetic Map for Tx631/Della.

The major QTL on chromosome 7 co-localized with the *Dw3* locus at ~58 Mbp in all three populations and in most all environments. This QTL was associated with morphological and mechanical traits. In the Tx623/Rio population the QTL explained 31.4-40.8%, 66.3-89.3%, 28.9-54.4%, and 80.1-81.3% of the genotypic variation for stiffness, rigidity, strength, and internode length with the high value allele coming from the parent Rio. In the Tx623/Della population the QTL on chromosome 7 explained 19.6-21.8%, 36.9%, 20.1-25%, and 22.3-29.9% of the genetic variation for stiffness, rigidity, strength, and internode length, respectively with the high value allele coming from Della. In the Tx631/Della population the QTL explained 23.9-24.5%, 65.2-24.8%, 15-25.3%, 20.1-25%, and 64.6-47.4% of the genetic variation for stiffness, rigidity, strength, and internode length, respectively with the high value allele coming from Della. This QTL was also associated with internode density in the Tx623/Rio population (the only population in which this trait was measured) and it explained 48% of the genotypic variation with the high value allele coming from the grain sorghum parent Tx623.

A second major QTL on chromosome 9 aligned with *Dw1* at ~57 Mbp in all three populations and in most environments. The QTL was found consistently to affect morphological and mechanical traits in all populations except in Tx631/Della were it only affected plant height. Nevertheless, the high value allele always came from the sweet sorghum parent except in the population Tx623/Rio were it was associated with internode density, and the high value allele came from the grain sorghum parent. Furthermore, a QTL was detected in all three populations in most environments on chromosome 1. For the Tx623/Rio population, morphological and mechanical traits were affected by this QTL

on chromosome 1 with the high value parent allele coming from the grain sorghum parent Tx623 (Table 6). While in Tx623/Della and Tx631/Della populations the QTL on chromosome 1 also affected mechanical and morphological traits with the high value allele for the mechanical traits coming from the sweet sorghum parent and the high value allele for the morphological traits including the geometric properties coming from the grain sorghum parent (Tables 7-8).

Other QTL for stiffness, strength, second moment of an area, section modulus, internode diameter, and internode length were detected on chromosome 4 in the Tx623/Rio and Tx623/Della populations at 55.5 Mbp and 63.7 Mpb respectively. A QTL affecting morphological and mechanical traits in Tx623/Rio and Tx631/Della was detected on chromosome 6 in CSE16, and it co-localized with *Ma1* at 40.3 Mbp (Thurber et al. 2013). These results indicate evidence of pleiotropic QTL for the mechanical and morphological QTL identified, consistent with the correlations between these traits (Table A2-4). Three other QTL were detected for individual populations only, at chromosome 2 and 5 for Tx631/Della and on chromosome 3 for Tx623/Rio. Quantitative trait loci analyses based on BLUEs for each trait adjusted for height (data not shown) were similar to QTL analysis based on BLUEs without height adjusted, indicating that the detected QTL are specific for the target traits.

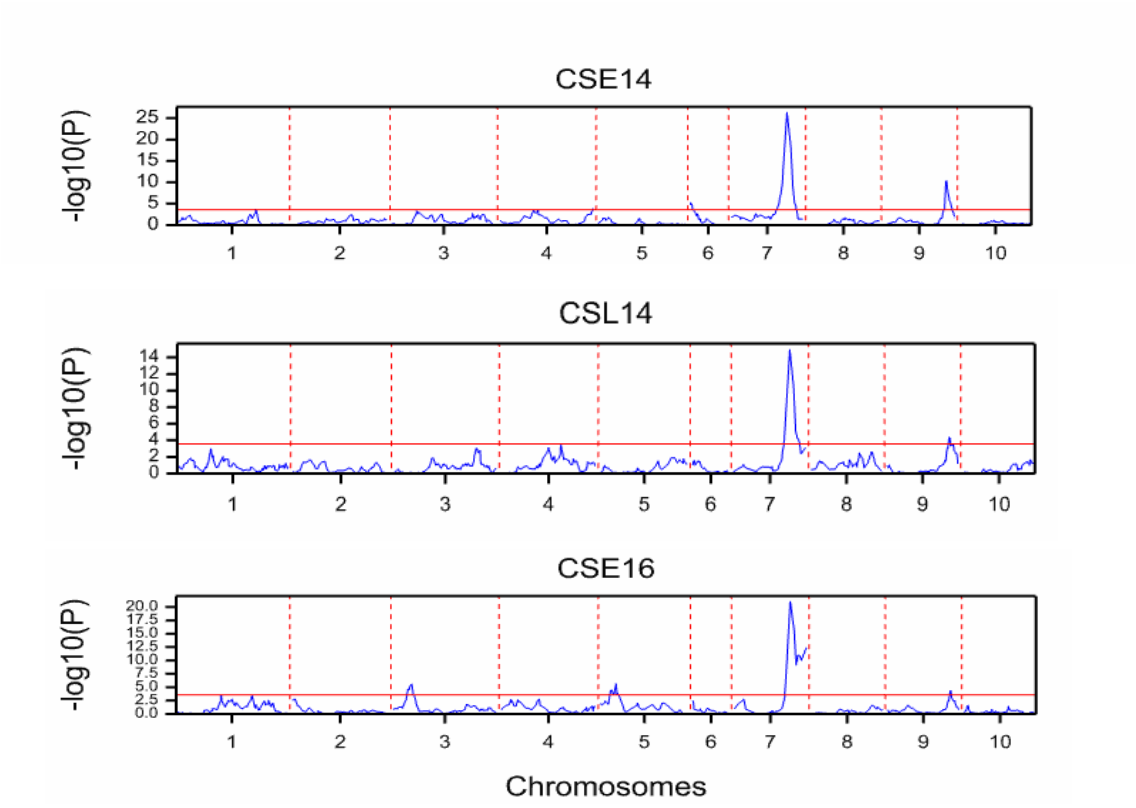

Fig. 13 Profile plot of the set of candidate QTLs following 1 round of SIM and 3 rounds of CIM, for Tx623/Rio in CSE14, CSL14, and CSE16 data. Step size=10cM.

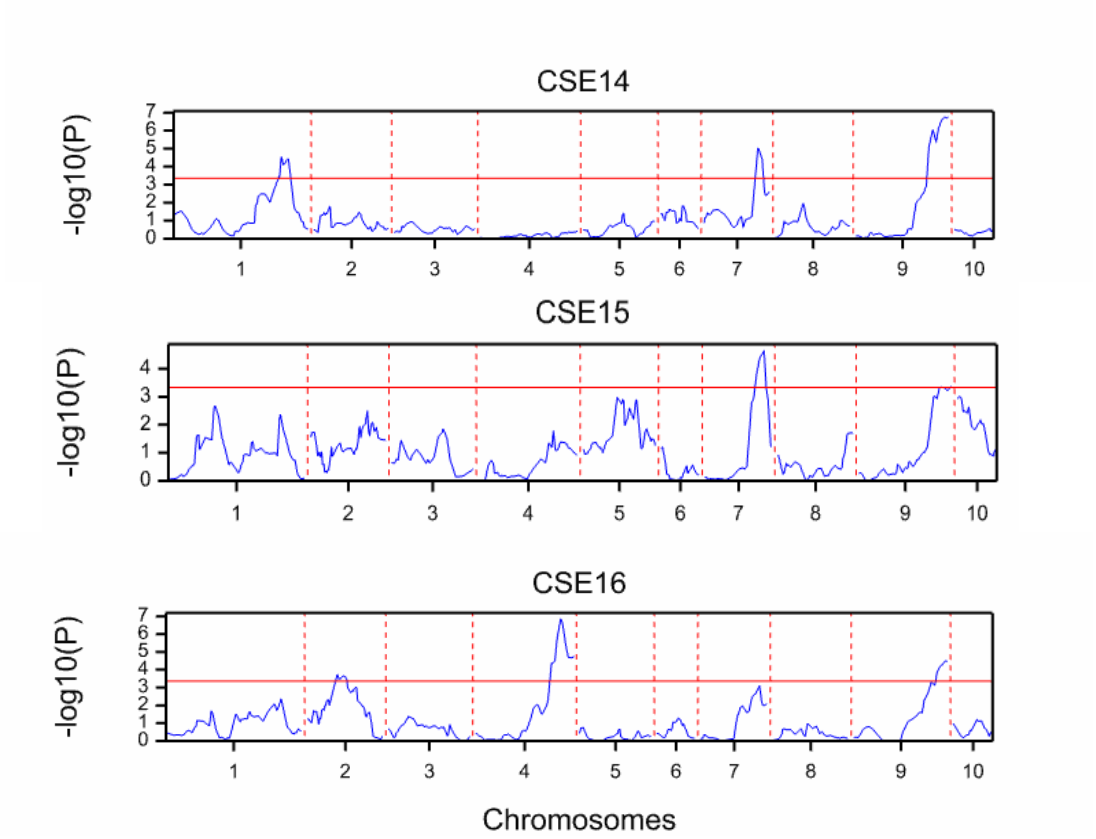

Fig. 14 Profile plot of the set of candidate QTLs following 1 round of SIM and 3 rounds of CIM, for Tx623/Della in CSE14, CSE15, and CSE16 data. Step size=10cM.

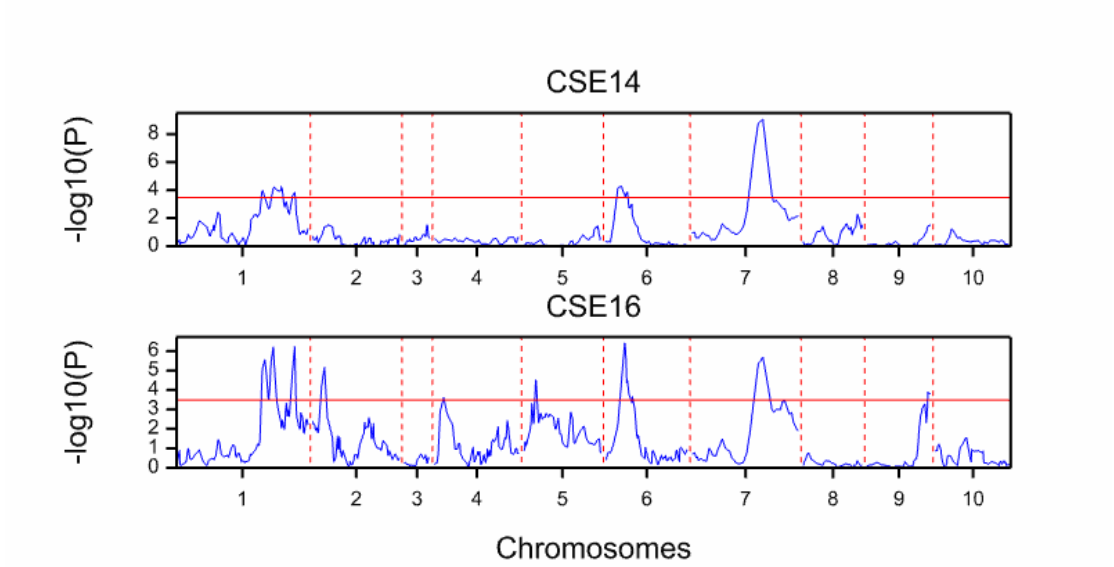

Fig. 15 Profile plot of the set of candidate QTLs following 1 round of SIM and 3 rounds of CIM, for Tx631/Della in CSE14 and CSE16 data. Step size=10cM.

Table 6 Multi-trait single environment Quantitative Trait Loci (QTL) detected for morphological and biomechanical traits for the RIL population Tx623/Rio.

Environment	QTL	Chrs	QTL Position (cM)	Effects [1]	High value allele [d]	%GV	s.e.
CSE14	E	1	150.07	0.205	Tx623	4.2	0.083
CSE14	Int_Density	1	150.07	0.2	Tx623	4	0.092
CSE14	Int_Length	1	150.07	0.144	Tx623	2.1	0.069
CSE14	Strength	1	150.07	0.169	Tx623	2.9	0.084
CSE16	EI	3	34.61	0.236	Tx623	5.6	0.096
CSE16	Int_Diam	3	34.61	0.231	Tx623	5.3	0.109
CSE16	Section_Modulus	3	34.61	0.218	Tx623	4.8	0.11
CSE14	E	4	175.69	0.27	Rio	7.3	0.082
CSE14	I	4	175.69	0.396	Tx623	15.7	0.098
CSE14	Int_Diam	4	175.69	0.363	Tx623	13.2	0.101
CSE14	Int_Length	4	175.69	0.195	Rio	3.8	0.068
CSE14	Section_Modulus	4	175.69	0.39	Tx623	15.2	0.098
CSE14	Strength	4	175.69	0.281	Rio	7.9	0.082
CSE14	E	6	0.56	0.166	Tx623	2.8	0.08
CSE14	Int_Length	6	0.56	0.172	Tx623	3	0.067
CSE14	E	7	105.3	0.639	Rio	40.8	0.113
CSE14	EI	7	105.3	0.932	Rio	86.8	0.1
CSE14	Int_Density	7	105.3	0.698	Tx623	48.7	0.126
CSE14	Int_Length	7	105.3	0.901	Rio	81.3	0.094
CSE14	Plant_Height	7	105.3	0.858	Rio	73.6	0.099
CSE14	Strength	7	105.3	0.737	Rio	54.4	0.114
CSL14	E	7	105.3	0.625	Rio	39	0.131
CSL14	EI	7	105.3	0.945	Rio	89.3	0.106
CSL14	Int_Density	7	105.3	0.693	Tx623	48.1	0.126
CSL14	Int_Length	7	105.3	0.895	Rio	80.1	0.112
CSL14	Plant_Height	7	105.3	1.011	Rio	100	0.096
CSL14	Strength	7	105.3	0.689	Rio	47.5	0.127
CSE16	E	7	105.3	0.56	Rio	31.4	0.189
CSE16	EI	7	105.3	0.814	Rio	66.3	0.164
CSE16	Int_Density	7	105.3	0.809	Tx623	65.4	0.178
CSE16	Int_Length	7	105.3	0.899	Rio	80.7	0.173
CSE16	Plant_Height	7	105.3	0.871	Rio	75.8	0.157
CSE16	Strength	7	105.3	0.538	Rio	28.9	0.181
CSE16	Int_Density	7	135.78	0.523	Rio	27.4	0.143
CSE14	E	9	118.54	0.185	Rio	3.4	0.082
CSE14	EI	9	118.54	0.305	Rio	9.3	0.072
CSE14	Int_Density	9	118.54	0.194	Tx623	3.7	0.091
CSE14	Int_Length	9	118.54	0.254	Rio	6.5	0.068
CSE14	Plant_Height	9	118.54	0.501	Rio	25.1	0.072
CSL14	EI	9	117.07	0.001	Rio	7.2	0.078
CSL14	Int_Density	9	117.07	0.007	Tx623	6.1	0.092
CSL14	Int_Length	9	117.07	0.004	Rio	5.6	0.082
CSL14	Plant_Height	9	117.07	0	Rio	12.1	0.07
CSL14	Strength	9	117.07	0.049	Rio	3.3	0.093
CSE16	EI	9	118.54	0.232	Rio	5.4	0.099
CSE16	I	9	118.54	0.277	Rio	7.7	0.114
CSE16	Int_Density	9	118.54	0.287	Tx623	8.2	0.108
CSE16	Int_Diam	9	118.54	0.279	Rio	7.8	0.113
CSE16	Plant_Height	9	118.54	0.367	Rio	13.5	0.095
CSE16	Section_Modulus	9	118.54	0.287	Rio	8.3	0.114

[1]Additive effects

Table 7 Multi-trait single environment Quantitative Trait Loci (QTL) detected for morphological and biomechanical traits for the RIL population Tx623/Della.

Environment	QTL	Chr.	QTL Position (cM) b	Effects[1]	High value allele	%GV	s.e.
CSE14	E	1	181.73	0.36	Della	13.3	0.11
CSE14	I	1	181.73	0.55	Tx623	29.7	0.12
CSE14	Int_diameter	1	181.73	0.58	Tx623	33.7	0.12
CSE14	Int_length	1	181.73	0.27	Della	7.3	0.10
CSE14	Section_modulus	1	181.73	0.56	Tx623	31.0	0.12
CSE14	Strength	1	181.73	0.27	Della	7.5	0.11
CSE16	E	4	142.18	0.31	Tx623	9.9	0.12
CSE16	Int_length	4	142.18	0.36	Tx623	12.9	0.11
CSE16	Strength	4	142.18	0.28	Tx623	7.8	0.13
CSE14	E	7	90.87	0.44	Della	19.6	0.11
CSE14	EI	7	90.87	0.61	Della	36.9	0.11
CSE14	Int_length	7	90.87	0.55	Della	29.9	0.10
CSE14	Plant_height	7	90.87	0.44	Della	19.1	0.12
CSE14	Strength	7	90.87	0.45	Della	20.1	0.12
CSE15	E	7	98.21	0.47	Della	21.8	0.14
CSE15	Int_length	7	98.21	0.47	Della	22.3	0.11
CSE15	Plant_height	7	98.21	0.41	Della	17.0	0.13
CSE15	Strength	7	98.21	0.50	Della	25.0	0.13
CSE14	E	9	145.65	0.30	Della	8.9	0.11
CSE14	EI	9	145.65	0.32	Della	10.5	0.10
CSE14	Int_length	9	145.65	0.45	Della	20.6	0.09
CSE14	Plant_height	9	145.65	0.44	Della	19.1	0.11
CSE14	Strength	9	145.65	0.24	Della	5.9	0.11
CSE15	E	9	156.16	0.38	Della	14.6	0.14
CSE15	Int_length	9	156.16	0.46	Della	20.8	0.11
CSE16	E	9	154.6	0.27	Della	7.0	0.13
CSE16	Int_length	9	154.6	0.48	Della	22.6	0.12
CSE16	Plant_height	9	154.6	0.36	Della	12.6	0.13

[1]Additive effects

Table 8 Multi-trait single environment Quantitative Trait Loci (QTL) detected for morphological and biomechanical traits for the RIL population Tx631/Della.

Environment	QTL	Chr.	QTL Position (cM)	Effects[1]	High value allele	%GV	s.e.
CSE14	E	1	179.86	0.539	Della	29	0.126
CSE14	EI	1	179.86	0.311	Della	9.7	0.127
CSE14	I	1	179.86	0.349	Tx631	12.2	0.131
CSE14	Int_diameter	1	179.86	0.321	Tx631	10.3	0.131
CSE14	Int_length	1	179.86	0.498	Della	24.8	0.118
CSE14	Section_modulus	1	179.86	0.345	Tx631	11.9	0.131
CSE14	Strength	1	179.86	0.519	Della	26.9	0.137
CSE14	EI	1	219.16	0.246	Tx631	6.1	0.122
CSE14	Int_length	1	219.16	0.232	Tx631	5.4	0.113
CSE16	E	1	202.41	0.261	Della	6.8	0.119
CSE16	Strength	1	202.41	0.292	Della	8.5	0.13
CSE16	E	1	247.27	0.324	Della	10.5	0.131
CSE16	I	1	247.27	0.489	Tx631	23.9	0.136
CSE16	Int_diameter	1	247.27	0.505	Tx631	25.5	0.132
CSE16	Section_modulus	1	247.27	0.503	Tx631	25.3	0.135
CSE16	Int_length	2	24.26	0.207	Della	4.3	0.1
CSE16	Plant_height	2	24.26	0.3	Della	9	0.106
CSE16	E	5	24.55	0.212	Della	4.5	0.097
CSE16	Plant_height	5	24.55	0.226	Della	5.1	0.105
CSE14	E	6	25.23	0.227	Tx631	5.2	0.111
CSE14	I	6	25.23	0.474	Della	22.5	0.115
CSE14	Int_diameter	6	25.23	0.379	Della	14.4	0.115
CSE14	Section_modulus	6	25.23	0.459	Della	21	0.115
CSE14	Strength	6	25.23	0.301	Tx631	9	0.12
CSE16	E	6	39.53	0.207	Tx631	4.3	0.095
CSE16	EI	6	39.53	0.279	Della	7.8	0.112
CSE16	I	6	39.53	0.42	Della	17.6	0.098
CSE16	Int_diameter	6	39.53	0.43	Della	18.5	0.096
CSE16	Section_modulus	6	39.53	0.421	Della	17.7	0.098
CSE16	Strength	6	39.53	0.251	Tx631	6.3	0.104
CSE14	E	7	147.35	0.489	Della	23.9	0.138
CSE14	EI	7	147.35	0.808	Della	65.2	0.139
CSE14	Int_length	7	147.35	0.804	Della	64.6	0.129
CSE14	Plant_height	7	147.35	0.546	Della	29.8	0.154
CSE14	Strength	7	147.35	0.387	Della	15	0.15
CSE16	E	7	137.82	0.495	Della	24.5	0.114
CSE16	EI	7	137.82	0.498	Della	24.8	0.134
CSE16	I	7	137.82	0.41	Tx631	16.8	0.118
CSE16	Int_diameter	7	137.82	0.382	Tx631	14.6	0.114
CSE16	Int_length	7	137.82	0.688	Della	47.4	0.116
CSE16	Plant_height	7	137.82	0.516	Della	26.6	0.123
CSE16	Section_modulus	7	137.82	0.403	Tx631	16.2	0.117
CSE16	Strength	7	137.82	0.503	Della	25.3	0.124
CSE16	Plant_height	9	127.05	0.346	Della	12	0.1

[1]Additive effects

Discussion

Future improvements in crop lodging resistance require a better understanding of how plants manage mechanical integrity and their acclimation and adaptation to their physical environment. In this study, we applied the knowledge of mechanics of an elastic longitudinal bar to dissect biomechanical traits in sorghum stems. The use of three different RIL populations allowed the dissection of the genetic basis of biomechanical traits and to concurrently validate the effects of the detected QTL in the different elite sweet and grain sorghum backgrounds. The three RIL populations were made from the cross between short grain parents carrying the recessive forms the dwarfing genes *dw1Dw2dw*3 and tall sweet sorghum parents homozygous for the dwarfing genes at all loci *Dw1Dw2Dw3*. Thus, the progeny always had a dominant *Dw2* allele, and were never be shorter than the grain sorghum parents. This permitted to study the effect of *Dw1* and *Dw3* and their association with mechanical traits. This study is the first in the literature to identify QTL for biomechanical traits and co-localize them with major dwarf genes in sorghum.

RILs performance and heritability of biomechanical traits

This study identified quantitative variation in all three populations for all morphological and biomechanical traits. There were significant genotypic differences among the RIL populations for biomechanical traits. The heritability estimates of biomechanical traits in each RIL population ranged from moderate to high within environments and much higher across environments. While there has been no previously

reported heritability for these mechanical traits in sorghum, a study in maize reported heritability of stalk strength related traits such as the maximum load exerted to breaking the internode, breaking moment, and critical stress was 81.0%, 79.0%, and 75.0%, respectively (Hu et al. 2013). Heritability was consistent across environments and populations.

Trait correlation

This study also demonstrated, through principal component analysis and trait correlations that the biomechanical properties stiffness, strength, and internode length tended to group together, indicating a correlation among morphological and biomechanical traits. These observations were consistent across populations and are also consistent with the theory of elastic mechanics, that holds that geometry influences material properties (Gere and Timoshenko 1984). This has also been reported in other studies where stem morphology largely affects mechanical properties (Von Forell et al. 2015; Gomez et al. 2017). In addition, the principal component analysis also indicates that, biomechanical traits and morphological traits are not independent of each other. Therefore, selection for mechanical traits may have foreseen consequences on plant size at this stage of the crop growth when the samples were harvested. Future research should investigate the indirect effects of morphology on biomechanical traits and vice-versa.

Genetic architecture of biomechanical traits

The genetic architecture of biomechanical traits in the three RIL populations appear to be quantitative and pleiotropic. A total of eight QTL located on chromosomes 1, 2, 3, 4, 5, 6, 7, and 9 affected morphological and mechanical traits. QTL detected on chromosomes 9, 7, and 1 were consistently associated with morphological and mechanical traits in all three populations in most environments, and were co-localized with *Dw1*, *Dw3*, and an uncharacterized locus, respectively. Furthermore, the high value allele for the mechanical traits for the two major QTL on chromosome 7 and 9 came from the sweet sorghum parent. These results indicate that dwarfing genes may affect the material properties of sorghum and ultimately their lodging resistance while also having a profound impact on the stems morphology and geometry.

The QTL on chromosome 1 were found in all three populations and were detected in most all environments and was associated with morphological and mechanical traits. All the high value alleles for this QTL in the Tx623/Rio population came from the grain parent. While in both Della populations the high value allele for the mechanical traits came from the sweet sorghum parent and the allele for morphological/geometric traits came from the grain parent except for internode length in the Tx631/Della population where it received alleles from both parents. It appears that the genomic regions responsible for mechanical and morphological traits in our study coincide with locations where dwarfing genes have been identified in sorghum. These results indicate that dwarfing genes in sorghum do, at least pleiotropically affect mechanical traits and lines homozygous for dominant *Dw* may have a positive impact on the mechanical stability of

plants. However, further analysis of the lines must be performed to confirm the impact of these alleles at a more quantitative level.

Previous studies in other cereal crops have identified QTL related to biomechanical traits. In rice, Ookawa et al. (2010) using chromosome segment substitution lines, identified an effective (QTL) for culm strength, on chromosome 1 of the cultivar Habataki, that was effective for increasing stem wall thickness designated as STRONG CULM1 (SCM1) and a second QTL affecting stem diameter on chromosome 6, designated as STRONG CULM2 (SCM2). SCM2 was found to be identical to ABERRANT PANICLE ORGANIZATION1 (APO1), a gene reported to control panicle structure. This gene enhanced culm strength and increased spikelet number due to the pleiotropic effects of this gene. The same group detected a QTL for section modulus using reciprocal chromosome segment substitution lines (CSSLs) derived from a cross between Koshihikari and Takanari (Ookawa et al. 2016). The study confirmed QTL in both genetic backgrounds on chromosomes 1, 5 and 6, suggesting that these QTLs are not affected by the genetic background. Since section modulus is associated with outer diameter and culm wall thickness, stem morphology and anatomy can have a profound impact on this trait. In maize, (Hu et al. 2013) looked at important stalk bending strength parameters of the fourth internode using a RIL population derived from B73 and Ce03005. The study detected two, three and two QTL explaining 22.4, 26.1 and 17.2 % of the genotypic variance for the maximum load exerted to breaking, breaking moment, and critical stress, respectively. These studies suggest that biomechanically related traits are pleiotropic which is consistent with the results of the current study.

Not all the QTL detected in this study were consistent across populations and environments. This lack of consistency may be the result of several factors, including differences in genetic background, population size, trait heritability, and map and marker density (Xu 2003; Beavis et al. 1991). At the same time, some of these factors may contribute to overestimation of the QTL in some of the traits. Nevertheless, known QTL were detected across populations and repeatedly in all environments and co-localized and with QTL associated with morphological and mechanical traits, indicating a high precision in phenotyping and expression of the trait.

Biomechanical properties co-located with dwarfing genes

Dwarfing genes have been important to reduce lodging in wheat and rice during the green revolution. In sorghum, four major dwarfing genes *Dw1-Dw4* have been described, and the combination of up to three major unlinked dwarfing genes, have been combined to reduce plant height by reducing internode length to increase lodging resistance and improve mechanized harvesting (Quinby and Karper 1953; Quinby 1974).

The QTL identified in the mapping populations co-localized with previously identified QTL for dwarfing genes *Dw1* and *Dw3*. Pleiotropic effects due to *Dw2* and *Dw3* have been reported to include panicle length, seed weight, and leaf area (Graham and Lessman 1966; Pereira and Lee 1995), seed weight, panicle size, tiller number, and leaf angle and for the latter (Pereira and Lee 1995; Cassady 1965; Truong et al. 2015). The gene corresponding to *Dw3* has been determined to encode an ABCB1 auxin efflux transporter (Multani et al. 2003). *Dw1* encodes a putative membrane protein (Hilley et al.

2016), that regulates cell proliferation activity in the internodes (Yamaguchi et al. 2016). In the same study, Yamaguchi et al. (2016) observed a synergistic interaction between *Dw1* and *Dw3*. The co-location of the QTL for mechanical traits with these dwarfing genes provides further support for the putative genetic association between mechanical stem traits and known morphological traits. However, it is still not clear how dwarfing genes may structurally affect the stem's mechanical properties.

Paolillo Jr and Niklas (1996) used near isogenic lines with different dosages of dwarfing genes (wild type, single dwarf, and double dwarf) to study the effect of the *Rht* alleles on the breaking strength and breaking stress of the first foliage leaves of wheat seedlings to assess the structural and material properties of *Rht* plants. The *Rht* alleles influence the microfibril orientation of the epidermal cells (Paolillo Jr 1995), and can ultimately affect their mechanical properties (Niklas 1992). They found that each increase of *Rht* dosage reduced the amount of fiber content and the proportional effect of fiber content on a blade strength, therefore reducing the capacity of the fiber strand wall area to sustain tensile loads. Like the *Dw* alleles in sorghum, the *Rht* alleles in wheat have multiple effects, reducing internode elongation (Pearce et al. 2011), altering the ability of coleoptiles to penetrate soil (Niklas and Paolillo Jr 1990), reducing amylase activity, and reducing lodging (Hedden 2003). The *Dw* genes in sorghum, like the *Rht* genes in wheat, may affect mechanical properties of plants by altering their chemistry of the cell wall matrix of fibers. Further experiments are needed to clarify to what extent *Dw* genes may affect mechanical properties.

Breeding for stem biomechanics in sorghum is likely to involve stem morphology characteristics. The ability of the plant stem to mechanically achieve stability is a result of their geometry or mechanical properties. While shorter plants may show reduced lodging, it is not because they are necessarily stronger but they invested in their geometry to reach mechanical stability. Furthermore, a study found that the *dw3* dwarfing gene was found to significantly reduced shoot biomass and affect grain yield (George-Jaeggli et al. 2011). Therefore, sorghum breeders should outline a breeding strategy when breeding for bioenergy sorghum hybrids, and restore these dominant dwarfing alleles to increase biomass and mechanical properties. Alternatively, sorghum breeders desiring short types should select for morphological/geometric traits to improve lodging resistance. For example, a QTL for internode density was identified with the high value allele coming from the grain sorghum parent. Stem internode density is known to predict strength (Gomez, et al., 2017, Submitted), and therefore can be used as indirect selection to improve lodging resistant dwarf varieties. Other QTL for second moment of an area and section modulus were identified on chromosome 1, with the high value allele coming from the grain sorghum parent. This confirms that grain sorghum invests its resources in the plants geometry to reach mechanical stability, and, thus breeders may select on a combination of geometry and density to improve grain sorghum. Future studies on mechanical properties of these complex composite structures at different, different growth stages, on different anatomical structures, and different hierarchical levels are warranted to provide insights into this complex phenomenology.

Implications for crop improvement programs targeting lodging resistance

Using biomechanical traits as a selection criterion in plant breeding has not been adopted, as it is still a new approach in crop improvement. However, our results identified moderate to high heritability for biomechanical traits for three RIL mapping populations. Consistent QTL were identified across populations and within environments that explained a large percent of the genetic variance and were consistent with the theory of material mechanics. Ultimately, the co-localization of mechanical traits with dwarfing genes sheds light on this important genetic system in plants that has had a profound and evolutionary changes by a single locus on which farmers and breeders have utilized. Our results demonstrate that *Dw* loci influences numerous biological features bearing on plant survival and reproductive success and provides insights for breeding lodging resistant cultivars.

CHAPTER IV

CONCLUSIONS

The field of plant breeding has always been interdisciplinary, promoting dialogue and collaborations with plant pathologists, biochemists, physiologists, molecular biologists, statisticians, and agronomists. However, interactions with new disciplines are becoming more common, such as mechanical engineering, material science, electrical engineering, and computer science are becoming more common as agriculture is becoming increasingly oriented to high-throughput methodologies. As such collaborations become increasingly common, new opportunities to obtain important experimental information appear, and new insights into crop evolution and new tools for crop improvement can be developed.

In the first study, we developed a high-throughput phenotyping platform capable of collecting important morphological and anatomical stem properties using an X-ray computed tomography. The use of CT on a diverse set of sorghum genotypes with a defined platform and image analysis pipeline was effective at predicting traits such as stem length, diameter, and pithiness ratio at the internode level. High-throughput phenotyping of stem traits using CT appears to be useful and feasible for use in an applied breeding program. We also explored the genetic basis of mechanical traits in sorghum. Mechanical traits in sorghum were found to be quantitative, pleiotropic, and heritable. Dwarfing alleles enhance mechanical traits in sorghum therefore breeders can co-select for morphological and biomechanical traits. This works is the first of its kind to apply X-ray computed

tomography in sorghum to predict morpho-anatomical traits and reveal the genetic architecture of mechanical traits in sorghum. It will help sorghum breeders increase genetic gain and maintain it by reducing stem lodging in tall forage, bioenergy, and sweet sorghum types.

REFERENCES

Alam, M.M., E.J. van Oosterom, A.W. Cruickshank, D.R. Jordan, and G.L. Hammer, 2016 Predicting Tillering of Diverse Sorghum Germplasm across Environments. *Crop Science*.

Andrade-Sanchez, P., M.A. Gore, J.T. Heun, K.R. Thorp, A.E. Carmo-Silva *et al.*, 2014 Development and evaluation of a field-based high-throughput phenotyping platform. *Functional Plant Biology* 41 (1):68-79.

Barker, J., N. Zhang, J. Sharon, R. Steeves, X. Wang *et al.*, 2016 Development of a field-based high-throughput mobile phenotyping platform. *Computers and Electronics in Agriculture* 122:74-85.

Bashford, L.L., J.W. Maranville, S.A. Weeks, and R. Campbell, 1976 Mechanical-Properties Affecting Lodging of Sorghum. *Transactions of the Asae* 19 (5):962-966.

Batz, J., M.A. Méndez-Dorado, and J.A. Thomasson, 2016 Imaging for high-throughput phenotyping in energy sorghum. *Journal of Imaging* 2 (1):4.

Beavis, W., D. Grant, M. Albertsen, and R. Fincher, 1991 Quantitative trait loci for plant height in four maize populations and their associations with qualitative genetic loci. *TAG Theoretical and Applied Genetics* 83 (2):141-145.

Berger, A., 2002 Bone mineral density scans. *BMJ: British Medical Journal* 325 (7362):484.

Berry, P., M. Sterling, J. Spink, C. Baker, R. Sylvester-Bradley *et al.*, 2004 Understanding and reducing lodging in cereals. *Advances in Agronomy* 84:217-271.

Blum, A., G. Golan, J. Mayer, and B. Sinmena, 1997 The effect of dwarfing genes on sorghum grain filling from remobilized stem reserves, under stress. *Field Crops Research* 52 (1):43-54.

Bucksch, A., A. Atta-Boateng, A.F. Azihou, D. Battogtokh, A. Baumgartner *et al.*, 2017 Morphological plant modeling: Unleashing geometric and topological potential within the plant sciences. *Frontiers in Plant Science* 8.

Carvalho, G., and W.L. Rooney, 2017 Assessment of Stalk Properties to Predict Juice Yield in Sorghum. *BioEnergy Research*:1-14.

Cassady, A., 1965 Effect of a single height (Dw) gene of sorghum on grain yield, grain yield components, and test weight. *Crop Science* 5 (5):385-388.

Chen, D., K. Neumann, S. Friedel, B. Kilian, M. Chen *et al.*, 2014 Dissecting the phenotypic components of crop plant growth and drought responses based on high-throughput image analysis. *The Plant Cell* 26 (12):4636-4655.

Cloetenes, P., R. Mache, M. Schlenker, and S. Lerbs-Mache, 2006 Quantitative phase tomography of Arabidopsis seeds reveals intrecellular void network. *Proceedings of the National Academy of Sciences* 103:1426-14630.

Comparini, D., T. Kihara, and T. Kawano, 2016 Uses of X-ray 3D-computed-tomography to monitor the development of garlic shooting inside the intact cloves. *Environmental Control in Biology* 54 (1):39-44.

Crook, M., and A. Ennos, 1994 Stem and root characteristics associated with lodging resistance in four winter wheat cultivars. *The Journal of Agricultural Science* 123 (02):167-174.

Crook, M., and A. Ennos, 1996 Mechanical Differences Between Free-standing and Supported Wheat Plants, Triticum aestivum L. *Annals of Botany* 77 (3):197-202.

Dhondt, S., H. Vanhaeren, D. Van Loo, V. Cnudde, and D. Inzé, 2010 Plant structure visualization by high-resolution X-ray computed tomography. *Trends in plant science* 15 (8):419-422.

Dutilleul, P., M. Lontoc-Roy, and S.O. Prasher, 2005 Branching out with a CT scanner. *TRENDS in plant Science* 9:411:412.

Esechie, H., J. Maranville, and W. Ross, 1977 Relationship of stalk morphology and chemical composition to lodging resistance in sorghum. *Crop Science* 17 (4):609-612.

Furbank, R.T., and M. Tester, 2011 Phenomics–technologies to relieve the phenotyping bottleneck. *Trends in plant science* 16 (12):635-644.

Gehan, M.A., and E.A. Kellogg, 2017 High-throughput phenotyping. *American Journal of Botany* 104 (4):505-508.

George-Jaeggli, B., D. Jordan, E. Van Oosterom, and G. Hammer, 2011 Decrease in sorghum grain yield due to the dw3 dwarfing gene is caused by reduction in shoot biomass. *Field Crops Research* 124 (2):231-239.

Gere, J., and S. Timoshenko, 1984 Mechanics of Materials, wadsworth. *Inc., Belmont, California*:351-355.

Gill, J.R., P.S. Burks, S.A. Staggenborg, G.N. Odvody, R.W. Heiniger *et al.*, 2014 Yield Results and Stability Analysis from the Sorghum Regional Biomass Feedstock Trial. *BioEnergy Research* 7 (3):1026-1034.

Gomez, F.E., A.H. Muliana, K.J. Niklas, and W.L. Rooney, 2017 Identifying Morphological and Mechanical Traits Associated with Stem Lodging in Bioenergy Sorghum (Sorghum bicolor). *BioEnergy Research*:1-13.

Graham, D., and K. Lessman, 1966 Effect of height on yield and yield components of two isogenic lines of Sorghum vulgare Pers. *Crop Science* 6 (4):372-374.

Hallauer, A.R., M.J. Carena, and J.d. Miranda Filho, 2010 *Quantitative genetics in maize breeding*: Springer Science & Business Media.

Hedden, P., 2003 The genes of the Green Revolution. *TRENDS in Genetics* 19 (1):5-9.

Hesse, L., S.T. Wagner, and C. Neinhuis, 2016 Biomechanics and functional morphology of a climbing monocot. *AoB Plants* 8:plw005.

Hilley, J., S. Truong, S. Olson, D. Morishige, and J. Mullet, 2016 Identification of Dw1, a regulator of sorghum stem internode length. *PLoS One* 11 (3):e0151271.

Hirano, K., A. Okuno, T. Hobo, R. Ordonio, Y. Shinozaki *et al.*, 2014 Utilization of stiff culm trait of rice smos1 mutant for increased lodging resistance. *PLoS One* 9 (7):e96009.

Hu, H., W. Liu, Z. Fu, L. Homann, F. Technow *et al.*, 2013 QTL mapping of stalk bending strength in a recombinant inbred line maize population. *Theor Appl Genet* 126 (9):2257-2266.

Kaminuma, E., T. Yoshizumi, T. Wada, M. Matsui, and T. Toyoda, 2008 Quantitative analysis of heterogenous spatial distribution of Arabidopsis leaf trichomes using micro X-ray computed tomography. *The Plant Journal* 56:471-482.

Karper, R., and J. Quinby, 1946 The history and evolution of Milo in the United States. *Agronomy Journal* 38 (5):441-453.

Keaveny, T.M., 2010 Biomechanical computed tomography—noninvasive bone strength analysis using clinical computed tomography scans. *Annals of the New York Academy of Sciences* 1192 (1):57-65.

Kosambi, D.D., 1943 The estimation of map distances from recombination values. *Annals of eugenics* 12 (1):172-175.

Lafond, J.A., L. Han, and P. Dutilleul, 2015 Concepts and analyses in the CT scanning of root systems and leaf canopies: A timely summary. *Frontiers in Plant Science* 6.

Lemloh, M.-L., A. Pohl, E. Weber, M. Zeiger, P. Bauer *et al.*, 2014 Structure-property relationships in mechanically stimulated Sorghum bicolor stalks. *Bioinspired Materials* 1 (1).

Li, H., and R. Durbin, 2010 Fast and accurate long-read alignment with Burrows–Wheeler transform. *Bioinformatics* 26 (5):589-595.

Malosetti, M., J.-M. Ribaut, and F.A. van Eeuwijk, 2013 The statistical analysis of multi-environment data: modeling genotype-by-environment interaction and its genetic basis. *Frontiers in physiology* 4.

Malosetti, M., J.M. Ribaut, M. Vargas, J. Crossa, and F.A. Van Eeuwijk, 2008 A multi-trait multi-environment QTL mixed model with an application to drought and nitrogen stress trials in maize (Zea mays L.). *Euphytica* 161 (1-2):241-257.

Metzner, R., A. Eggert, D. van Dusschoten, D. Pflugfelder, S. Gerth *et al.*, 2015 Direct comparison of MRI and X-ray CT technologies for 3D imaging of root systems in soil: potential and challenges for root trait quantification. *Plant Methods* 11 (1):17.

Morishige, D.T., P.E. Klein, J.L. Hilley, S.M.E. Sahraeian, A. Sharma *et al.*, 2013 Digital genotyping of sorghum–a diverse plant species with a large repeat-rich genome. *BMC Genomics* 14 (1):448.

Mullet, J., D. Morishige, R. McCormick, S. Truong, J. Hilley *et al.*, 2014 Energy sorghum--a genetic model for the design of C4 grass bioenergy crops. *J Exp Bot* 65 (13):3479-3489.

Multani, D.S., S.P. Briggs, M.A. Chamberlin, J.J. Blakeslee, A.S. Murphy *et al.*, 2003 Loss of an MDR transporter in compact stalks of maize br2 and sorghum dw3 mutants. *Science* 302 (5642):81-84.

Murray, S.C., A. Sharma, W.L. Rooney, P.E. Klein, J.E. Mullet *et al.*, 2008 Genetic improvement of sorghum as a biofuel feedstock: I. QTL for stem sugar and grain nonstructural carbohydrates. *Crop Science* 48 (6):2165-2179.

Niklas, K.J., 1992 *Plant biomechanics: an engineering approach to plant form and function*: University of Chicago press.

Niklas, K.J., and D.J. Paolillo Jr, 1990 Biomechanical and morphometric differences in Triticum aestivum seedlings differing in Rht gene-dosage. *Annals of Botany* 65 (4):365-377.

Niklas, K.J., and H.-C. Spatz, 2012 *Plant physics*: University of Chicago Press.

Okuno, A., K. Hirano, K. Asano, W. Takase, R. Masuda *et al.*, 2014 New approach to increasing rice lodging resistance and biomass yield through the use of high gibberellin producing varieties. *PLoS One* 9 (2):e86870.

Oladokun, M.A., and A.R. Ennos, 2006 Structural development and stability of rice Oryza sativa L. var. Nerica 1. *J Exp Bot* 57 (12):3123-3130.

Ookawa, T., R. Aoba, T. Yamamoto, T. Ueda, T. Takai *et al.*, 2016 Precise estimation of genomic regions controlling lodging resistance using a set of reciprocal chromosome segment substitution lines in rice. *Scientific Reports* 6.

Ookawa, T., T. Hobo, M. Yano, K. Murata, T. Ando *et al.*, 2010 New approach for rice improvement using a pleiotropic QTL gene for lodging resistance and yield. *Nature communications* 1:132.

Pajor, R., A. Fleming, C.P. Osborne, S.A. Rolfe, C.J. Sturrock *et al.*, 2013 Seeing space: visualization and quantification of plant leaf structure using X-ray micro-computed tomography. *Journal of Experimental Botany*:385-390.

Paolillo Jr, D., 1995 The net orientation of wall microfibrils in the outer periclinal epidermal walls of seedling leaves of wheat. *Annals of Botany* 76 (6):589-596.

Paolillo Jr, D.J., and K.J. Niklas, 1996 Effects of Rht-dosage on the breaking strength of wheat seedling leaves. *American Journal of Botany*:567-572.

Paterson, A.H., J.E. Bowers, R. Bruggmann, I. Dubchak, J. Grimwood *et al.*, 2009 The Sorghum bicolor genome and the diversification of grasses. *Nature* 457 (7229):551-556.

Pearce, S., R. Saville, S.P. Vaughan, P.M. Chandler, E.P. Wilhelm *et al.*, 2011 Molecular characterization of Rht-1 dwarfing genes in hexaploid wheat. *Plant Physiology* 157 (4):1820-1831.

Pereira, M., and M. Lee, 1995 Identification of genomic regions affecting plant height in sorghum and maize. *TAG Theoretical and Applied Genetics* 90 (3):380-388.

Piepho, H.P., J. Möhring, T. Schulz-Streeck, and J.O. Ogutu, 2012 A stage-wise approach for the analysis of multi-environment trials. *Biometrical Journal* 54 (6):844-860.

Piñera-Chavez, F., P. Berry, M. Foulkes, G. Molero, and M. Reynolds, 2016 Avoiding lodging in irrigated spring wheat. II. Genetic variation of stem and root structural properties. *Field Crops Research* 196:64-74.

Quinby, J., and R. Karper, 1953 Inheritance of height in sorghum. *Inheritance of height in sorghum.*

Quinby, J.R., 1974 Sorghum improvement and the genetics of growth.

Robertson, D.J., M. Julias, S.Y. Lee, and D.D. Cook, 2017 Maize Stalk Lodging: Morphological Determinants of Stalk Strength. *Crop Science* 57 (2):926-934.

Rooney, W.L., J. Blumenthal, B. Bean, and J.E. Mullet, 2007 Designing sorghum as a dedicated bioenergy feedstock. *Biofuels, Bioproducts and Biorefining* 1 (2):147-157.

Rowe, N.P., S. Isnard, F. Gallenmüller, and T. Speck, 2006 Diversity of mechanical architectures in climbing plants: an ecological perspective. *Ecology and biomechanics: A mechanical approach to the ecology of animals and plants*:35-59.

Schulgasser, K., and A. Witztum, 1997 On the strength of herbaceous vascular plant stems. *Annals of Botany* 80 (1):35-44.

Speck, T., and I. Burgert, 2011 Plant stems: functional design and mechanics. *Annual review of materials research* 41:169-193.

Stuppy, W.H., J.A. Maisano, M.W. Colbert, P.J. Rudall, and T.B. Rowe, 2003 Three-dimensional analysis of plant structure using high-resolution X-ray computed tomography. *Trends in plant science* 8 (1):2-6.

Thurber, C.S., J.M. Ma, R.H. Higgins, and P.J. Brown, 2013 Retrospective genomic analysis of sorghum adaptation to temperate-zone grain production. *Genome Biology* 14 (6):R68.

Tracy, S.R., J.F. Gómez, C.J. Sturrock, Z.A. Wilson, and A.C. Ferguson, 2017 Non-destructive determination of floral staging in cereals using X-ray micro computed tomography (μCT). *Plant Methods* 13 (1):9.

Truong, S.K., R.F. McCormick, W.L. Rooney, and J.E. Mullet, 2015 Harnessing Genetic Variation in Leaf Angle to Increase Productivity of Sorghum bicolor. *Genetics* 201 (3):1229-1238.

Van Ooijen, J.W., and R. Voorrips, 2001 JoinMap® 3.0, Software for the calculation of genetic linkage maps. *Plant research international, Wageningen*:1-51.

Von Forell, G., D. Robertson, S.Y. Lee, and D.D. Cook, 2015 Preventing lodging in bioenergy crops: a biomechanical analysis of maize stalks suggests a new approach. *J Exp Bot* 66 (14):4367-4371.

Wagner, S.T., S. Isnard, N.P. Rowe, M.-S. Samain, C. Neinhuis *et al.*, 2012 Escaping the lianoid habit: evolution of shrub-like growth forms in Aristolochia subgenus Isotrema (Aristolochiaceae). *American Journal of Botany* 99 (10):1609-1629.

Watanabe, K., W. Guo, K. Arai, H. Takanashi, H. Kajiya-Kanegae *et al.*, 2017 High-Throughput Phenotyping of Sorghum Plant Height Using an Unmanned Aerial Vehicle and Its Application to Genomic Prediction Modeling. *Frontiers in Plant Science* 8.

Xu, S., 2003 Theoretical basis of the Beavis effect. *Genetics* 165 (4):2259-2268.

Yamaguchi, M., H. Fujimoto, K. Hirano, S. Araki-Nakamura, K. Ohmae-Shinohara *et al.*, 2016 Sorghum Dw1, an agronomically important gene for lodging resistance, encodes a novel protein involved in cell proliferation. *Scientific Reports* 6.

APPENDIX

Table A-1 Sorghum genotypes used in this study with their respective set, maturity, type, and end-use.

Genotype	Set	Maturity	Type	End-Use
B.Tx623	1	PI	Inbred Line	Grain
B.Tx645	1	PI	Inbred Line	Grain
Della	1	PI	Inbred Line	Biofuel
Tx14323	1	PI	Inbred Line	Forage
Tx15323	1	PI	Inbred Line	Forage
R.07007	1	PS	Inbred Line	Biomass
Tx13320	1	PS	Hybrid	Forage/Biofuel
M81E	1	PS	Inbred Line	Biofuel
Rio	1	PS	Inbred Line	Biofuel
Tx13321	1	PS	Hybrid	Biofuel
Tx13322	1	PS	Hybrid	Biofuel
ATx623/R07007	1	PS	Hybrid	Biomass
ATx645/Tx14323	1	PS	Hybrid	Forage/Biomass
R.11434	1	PS	Inbred Line	Biomass
R.11438	1	PS	Inbred Line	Biomass
R.10030	1	PS	Inbred Line	Biomass
R.10135	1	PS	Inbred Line	Biomass
GRASSL	1	PS	Inbred Line	Biomass
GIZA114	1	PS	Inbred Line	Biomass
(GIZA114/Umbrella)-101	2			
(GIZA114/Umbrella)-102	2			
(GIZA114/Umbrella)-103	2			
(GIZA114/Umbrella)-104	2			
(GIZA114/Umbrella)-105	2			
(GIZA114/Umbrella)-111	2			
(GIZA114/Umbrella)-112	2			
(GIZA114/Umbrella)-113	2			
(GIZA114/Umbrella)-114	2			
(GIZA114/Umbrella)-115	2			

Table A-2 Correlation of traits to PCA axes for Tx623.Rio using BLUEs from combined analysis

	Prin1	Prin2	Prin3	Prin4	Prin5	Prin6	Prin7	Prin8	Prin9
PHE	0.70	0.63	0.06	0.02	-0.32	0.02	0.00	0.00	0.00
ILE	0.90	0.38	-0.06	-0.17	0.07	0.02	0.09	0.01	0.00
IDI	-0.63	0.77	0.02	0.05	0.05	0.01	0.03	-0.07	0.00
IDE	-0.66	-0.29	0.69	-0.08	-0.05	0.00	0.03	0.00	0.00
I	-0.64	0.76	0.03	0.04	0.05	0.05	-0.01	0.04	-0.01
SMO	-0.63	0.78	0.02	0.04	0.04	0.02	0.00	0.02	0.01
E	0.96	0.03	0.19	-0.08	0.11	0.13	-0.05	-0.02	0.00
STR	0.91	-0.01	0.22	0.34	0.07	-0.01	0.03	0.01	0.00
EI	0.69	0.67	0.20	-0.10	0.08	-0.13	-0.04	0.00	0.00

Table A-3 Correlation of traits to PCA axes for Tx623.Della using BLUEs from combined analysis

	Prin1	Prin2	Prin3	Prin4	Prin5	Prin6	Prin7	Prin8	Prin9
PHE	-0.19	0.95	0.04	-0.09	-0.22	0.01	-0.02	0.00	0.00
ILE	-0.67	0.71	0.00	-0.15	0.08	0.08	0.08	0.00	0.00
IDI	0.87	0.48	0.03	0.07	0.03	0.04	-0.01	0.07	0.00
I	0.87	0.46	0.07	0.14	0.02	0.06	0.00	-0.04	-0.01
SMO	0.87	0.48	0.06	0.10	0.02	0.03	0.01	-0.02	0.02
E	-0.96	0.17	0.18	0.02	0.07	0.10	-0.08	0.00	0.00
STR	-0.92	-0.01	0.23	0.32	-0.05	-0.02	0.04	0.01	0.00
EI	-0.09	0.95	0.22	-0.05	0.10	-0.15	-0.02	0.00	0.00

Table A-4 Correlation of traits to PCA axes for Tx631.Della using BLUEs from combined analysis

	Prin1	Prin2	Prin3	Prin4	Prin5	Prin6	Prin7	Prin8
PHE	0.36	0.88	-0.17	0.23	0.01	0.03	0.00	0.00
ILE	0.81	0.54	-0.14	-0.15	0.09	-0.08	0.02	0.00
IDI	-0.86	0.49	0.10	0.00	-0.01	-0.01	0.12	0.00
I	-0.87	0.47	0.12	-0.01	0.08	0.02	-0.05	-0.01
SMO	-0.87	0.48	0.09	-0.02	0.05	-0.01	-0.04	0.01
E	0.98	0.07	0.13	-0.05	0.08	0.12	0.03	0.00
STR	0.94	0.04	0.30	0.13	0.00	-0.08	-0.01	0.00
EI	0.44	0.88	0.07	-0.13	-0.13	0.02	-0.03	0.00

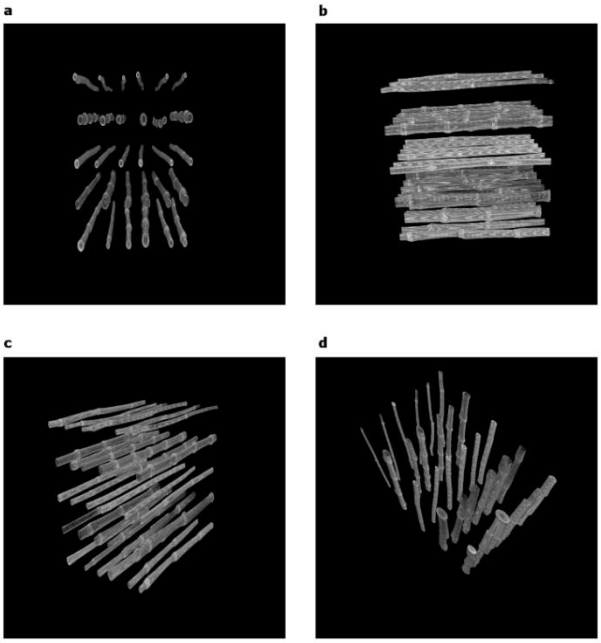

Fig. A-1 X-ray computed tomography of sorghum stems arranged in platform used in this study.

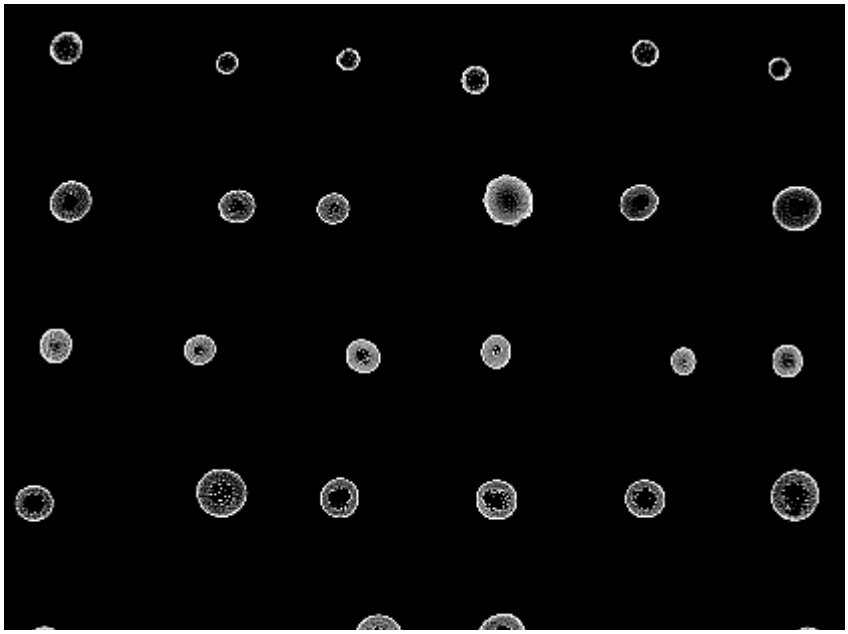

Fig. A-2 Cross sections of 30 sorghum stems during one run of CT scanning showing different attenuation values.